American Journal of Pathology, Vol. 164, No. 1, January 2004

Role of Ubiquitin Carboxy Terminal Hydrolase-L1 in Neural Cell Apoptosis Induced by Ischemic Retinal Injury *in Vivo*

Takayuki Harada,*† Chikako Harada,*† Yu-Lai Wang,* Hitoshi Osaka,*‡ Kazuhito Amanai,† Kohichi Tanaka,†‡ Shuichi Takizawa,* Rieko Setsuie,*§ Mikako Sakurai,*§ Yae Sato,*§ Mami Noda,§ and Keiji Wada*

From the Department of Degenerative Neurological Diseases, National Institute of Neuroscience, National Center of Neurology and Psychiatry, Kodaira, Tokyo; Laboratory of Molecular Neuroscience,† School of Biomedical Science and Medical Research Institute, Tokyo Medical and Dental University, Tokyo; Precursory Research for Embryonic Science and Technology (PRESTO),‡ Japan Science and Technology Corporation (JST), Kawaguchi, Saitama; Laboratory of Pathophysiology,§ Graduate School of Pharmaceutical Sciences, Kyushu University, Higashi-ku, Fukuoka, Japan*

Ubiquitin is thought to be a stress protein that plays an important role in protecting cells under stress conditions; however, its precise role is unclear. Ubiquitin expression level is controlled by the balance of ubiquitinating and deubiquitinating enzymes. To investigate the function of deubiquitinating enzymes on ischemia-induced neural cell apoptosis *in vivo*, we analyzed gracile axonal dystrophy (*gad*) mice with an exon deletion for ubiquitin carboxy terminal hydrolase-L1 (UCH-L1), a neuron-specific deubiquitinating enzyme. In wild-type mouse retina, light stimuli and ischemic retinal injury induced strong ubiquitin expression in the inner retina, and its expression pattern was similar to that of UCH-L1. On the other hand, *gad* mice showed reduced ubiquitin induction after light stimuli and ischemia, whereas expression levels of antiapoptotic (Bcl-2 and XIAP) and prosurvival (brain-derived neurotrophic factor) proteins that are normally degraded by an ubiquitin-proteasome pathway were significantly higher. Consistently, ischemia-induced caspase activity and neural cell apoptosis were suppressed ~70% in *gad* mice. These results demonstrate that UCH-L1 is involved in ubiquitin expression after stress stimuli, but excessive ubiquitin induction following ischemic injury may rather lead to neural cell apoptosis *in vivo*. (Am J Pathol 2004, 164:59–64)

The small 76 amino acid protein ubiquitin plays a critical role in many cellular processes, including cell cycle control, transcriptional regulation, and synaptic development.[1,2] Although ubiquitin has been identified as a heat shock- and stress-regulated protein in several kinds of cells,[3,4] recent studies have shown that ubiquitin promotes either cell survival or apoptosis, depending on the stage of cell development or other cellular factors.[5–8] Ubiquitin expression level is controlled by the balance of ubiquitinating enzymes: ubiquitin-activating (E1), ubiquitin-conjugating (E2), ubiquitin-ligase (E3) enzymes, and deubiquitinating enzymes (DUBs). DUBs are subdivided into ubiquitin carboxy terminal hydrolases (UCHs) and ubiquitin-specific proteases (UBPs). Mammalian UCHs, UCH-L1, and UCH-L3 are both small proteins of ~220 amino acids that share >40% amino acid sequence identity.[9] However, the distribution of these isozymes is quite distinct in that UCH-L3 is distributed ubiquitously while UCH-L1 is selectively expressed in neuronal cells and in the testis/ovary.[9,10] UCH-L1 constitutes ~5% of the brain's total soluble protein, which demonstrates a possibility that it plays a major role in neuronal cell function.[11] Indeed, UCH-L1 is a constituent of cellular aggregates that are indicative of neurodegenerative disease, such as Lewy bodies in Parkinson's disease.[12] Furthermore, an isoleucine to methionine substitution at amino acid 93 of UCH-L1 is reported in a family with a dominant form of Parkinson's disease.[13] Recently, we found a UCH-L1 gene exon deletion in mice that causes gracile axonal dystrophy (*gad*), a recessive neurodegenerative disease.[14] These examples of neurodysfunction from UCH-L1 mutations in both humans and mice prompted us to investigate the function of UCH-L1 in ischemia-induced neuronal cell apoptosis. For this purpose, we evaluated the extent of ischemic injury in wild-type and *gad* mice retina. The retina was chosen as a model be-

Supported by grants from the Organization for Pharmaceutical Safety and Research, Japan Science and Technology Cooperation, the Ministry of Health, Labor and Welfare of Japan, and the Ministry of Education, Culture, Sports, Science and Technology of Japan.

C. H. was supported by the Japan Society for the Promotion of Science for Young Scientists.

Accepted for publication September 10, 2003.

Address reprint requests to Keiji Wada, M.D., Ph.D., Department of Degenerative Neurological Diseases, National Institute of Neuroscience, NCNP, 4-1-1 Ogawahigashi, Kodaira, Tokyo 187-8502, Japan. E-mail: wada@ncnp.go.jp.

cause it is a highly organized neural tissue. In addition, its layered construction is suitable for analysis of cell type-specific biological response against diverse stimuli.[15–18] Here, we show that the absence of UCH-L1 partially prevents ischemia-induced retinal cell apoptosis and propose its possible mechanisms.

Materials and Methods

Animals

We used homozygous *gad* mice[14] and their wild-type littermates between postnatal days 35 and 56. The *gad* mouse was found in the F2 offspring of CBA and RFM inbred strain mice and has been maintained by brother-sister mating for more than 10 years.[19] Mice were maintained and propagated at the National Institute of Neuroscience, National Center of Neurology and Psychiatry (Japan). Experiments using the mice were approved by the Animal Investigation Committee of the Institute. The animals were housed in a room with controlled temperature and fixed lighting schedule. Light intensity inside the cages ranged from 100 to 200 lux. For the analysis of light stress, the pupils were dilated with 0.5% phenylephrinezhydrochloride and 0.5% tropicamide, and the mice were exposed to 800~1300 lux of white fluorescent light for 30 minutes. Animals for negative controls were dark-adapted for 12 hours, and sacrificed under dim red light.

Immunohistochemistry

Animals were anesthetized with diethylether and perfused transcardially with saline, followed by 4% paraformaldehyde in 0.1 mol/L phosphate buffer containing 0.5% picric acid at room temperature. The eyes were removed and postfixed overnight in the same fixative at 4°C and embedded in paraffin wax. The posterior part of the eyes were sectioned saggitally at 7-μm thickness through the optic nerve, mounted and stained with hematoxylin and eosin. For immunohistochemical staining, the sections were incubated with phosphate-buffered saline (PBS) containing 10% normal donkey serum for 30 minutes at room temperature. They were then incubated overnight with a rabbit polyclonal antibody against ubiquitin (1:600; Chemicon, Temecula, CA) or mouse monoclonal antibody against UCH-L1 (1:200; Medac, Wedel, Germany). They were then visualized with fluorescein isothiocyanate (FITC)-conjugated goat anti-rabbit or anti-mouse IgG (Jackson Immunoresearch, West Grove, PA), respectively. The sections were examined by a confocal laser scanning microscope (Olympus, Tokyo, Japan).

Histology and Morphometric Studies

Ischemia was achieved and the animals were sacrificed as previously described.[16,17] Briefly, we instilled sterile saline into the anterior chamber of the left eye at 150 cm H_2O pressure for 15 minutes while the right eye served as a non-ischemic control. The animals were sacrificed 1 or 7 days after reperfusion, and eyes were enucleated for histological and morphometric studies. The posterior part of the eyes was sectioned sagittally at 7-μm thickness through the optic nerve, mounted and stained with hematoxylin and eosin. Ischemic damage after 7 days was quantified in two ways. First, the thickness of the inner retinal layer (IRL) [from the ganglion cell layer (GCL) to the inner nuclear layer (INL)] was measured with a calibrated reticle at ×80. Second, in the same sections, the number of cells in the GCL was counted from one ora serrata through the optic nerve to the other ora serrata. The changes of the number of ganglion cells after ischemia were expressed in ratio compared with the non-ischemic fellow eyes.

TUNEL Staining

Sections were incubated in 0.26 U/μl TdT in the supplied 1X buffer (Invitrogen, Carlsbad, CA), and 20 μmol/L biotinylated-16-dUTP (Roche, Basel, Switzerland) for 60 minutes at 37°C. Sections were washed three times in PBS (pH 7.4) and blocked for 30 minutes with 2% bovine serum albumin in PBS (pH 7.4). The sections were then incubated with FITC-coupled streptavidin (Jackson Immunoresearch), diluted 1:100 in PBS for 30 minutes, and examined with a confocal laser scanning microscope (Olympus).

Quantification of Retinal Cell Apoptosis and Caspase Activities

A mouse retina 1 day after ischemia was homogenized in 100 μl PBS containing 1 mmol/L phenylmethyl sulfonyl fluoride and centrifuged at 15,000 × *g* for 10 minutes. A portion of supernatant was used to quantify protein concentration, and the rest was processed for assays. Retinal cell apoptosis was quantified using the Cell Death ELISA kit (Roche). Caspase-1- and caspase-3-like activities were measured using caspase-1 and caspase-3 Colorimetric Assay Kits (Bio-vision, Mountain View, CA), respectively.

Western Blot Analysis

Western blots were performed as previously reported.[14] Five micrograms of total protein were loaded per lane. Primary antibodies used were Bcl-2 (1:500), Bcl-xL (1:500), XIAP (1:500) (all from Transduction Laboratories, Franklin Lakes, NJ), phosphorylated cyclic AMP responsive element-binding protein (PCREB) (1:500; Upstate Biotechnology, Waltham, MA) and brain-derived neurotrophic factor (BDNF) (1:500; Santa Cruz Biotechnology, Santa Cruz, CA). Blots were further incubated with an anti-mouse or rabbit IgG-horseradish peroxidase conjugate (1:10000; Chemicon). The Super Signal detection kit (Pierce, Rockford, IL) was used for visualization of immunoreactive bands.

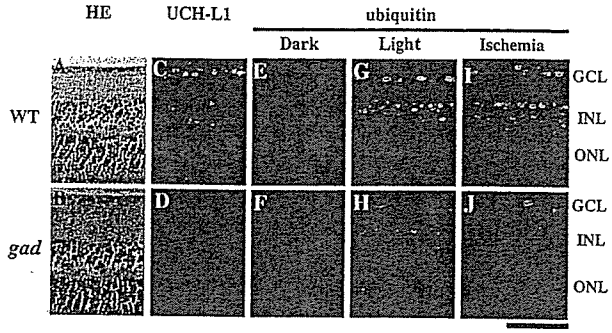

Figure 1. Functional loss of UCH-L1 decreases light- and ischemia-induced ubiquitin induction *in vivo*. Hematoxylin and eosin (HE) staining (**A** and **B**), immunostaining of UCH-L1 (**C** and **D**), immunostaining of ubiquitin in dark-reared (**E** and **F**), light-stressed (**G** and **H**) and ischemic (**I** and **J**) retina in wild-type (**A**, **C**, **E**, **G**, and **I**) and *gad* (**B**, **D**, **F**, **H**, and **J**) mice. Retinal structure is normal (**B**), but stress-induced ubiquitin induction is reduced (**H** and **J**) in *gad* mice. For the analysis of light stress (**G** and **H**), mice were exposed to 800 to 1300 lux of light for 30 minutes. Animals for negative controls were dark-adapted for 12 hours, and sacrificed under dim red light (**E** and **F**). Ischemic retina was prepared 1 day after ischemic injury (**I** and **J**). Bar, 50 μm.

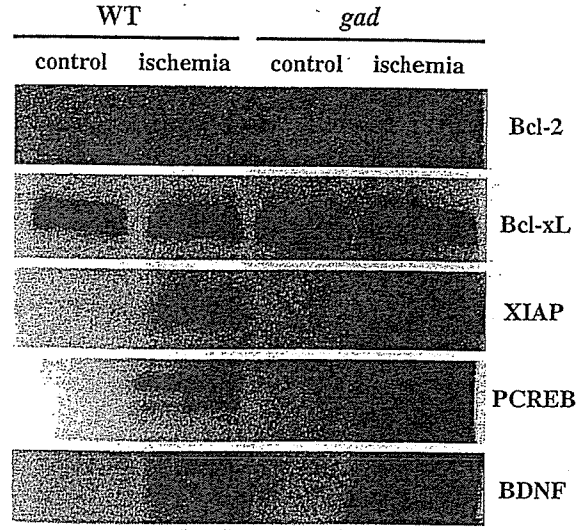

Figure 2. Immunoblot analysis of antiapoptotic and prosurvival proteins after ischemic injury. Five micrograms of total protein were prepared from whole retinas before (control) and 1 day after ischemic injury (ischemia). Representative image of four independent experiments are shown.

Results

Effect of UCH-L1 on Retinal Structure and Ubiquitin Expression

To determine the effect of UCH-L1 on retinal morphology, we examined the retinal tissue of *gad* mice with a UCH-L1 gene exon deletion.[14] Retinal structure in *gad* mice (Figure 1B) was normal compared with wild-type mice (Figure 1A). UCH-L1-like immunoreactivity was observed in the ganglion cell layer (GCL) and the inner nuclear layer (INL) in wild-type mice (Figure 1C) but was absent in *gad* mice (Figure 1D). Since ubiquitin is thought to be a stress protein,[1,20] we first examined the effect of the common oxidative stress for eye tissues, light stimuli, on ubiquitin induction.[20] Interestingly, ubiquitin was almost absent in both groups of animals, following dark adaptation (Figure 1, E and F). However, light stimuli strongly induced ubiquitin expression in the GCL and INL in wild-type mice (Figure 1G) but its induction level was very low in *gad* mice (Figure 1H). Ubiquitin expression pattern in wild-type mice was similar to that of UCH-L1 (Figure 1C). We next examined the effect of ischemia, severe oxidative stress,[21,22] on ubiquitin induction. As with light stimuli, ischemia induced strong ubiquitin expression in the GCL and INL (Figure 1I) and its induction was suppressed in *gad* mice (Figure 1J). These results demonstrate that retinal UCH-L1 plays an important role in ubiquitin induction[11] and *gad* mice retina is a useful model to investigate the effects of UCH-L1 on ischemic injury *in vivo*.

Effect of UCH-L1 on Antiapoptotic and Prosurvival Protein Expressions Following Ischemic Injury

The ubiquitin-proteasome pathway might be involved in non-neural cell apoptosis because this pathway can degradate antiapoptotic proteins such as Bcl-2 and XIAP *in vitro*.[5–8] To determine whether this is true for retinal cell apoptosis *in vivo*, we examined their protein expression levels in ischemic retinas (Figure 2). Ischemia-induced Bcl-2 protein level in *gad* mice was substantially higher than that of wild-type mice. Bcl-xL proteins (antiapoptotic member in the Bcl-2 family)[23,24] were examined at the same time as a control, but no obvious alternations were noted. On the other hand, XIAP protein[25,26] expression was apparently higher in *gad* mice. In addition to oxidative stress, ischemia induces calcium influx in neurons and triggers phosphorylation of cyclic AMP responsive element-binding protein (CREB).[27] PCREB can activate transcription of trophic factor proteins, such as BDNF, by binding to a critical calcium response element.[27] Since CREB is degraded by a ubiquitin-proteasome pathway by a phosphorylation-dependent mechanism,[28] we hypothesized a similar degradative pathway for CREB in ischemic retina. In wild-type mice, ischemia increased PCREB, but its expression level was much higher in *gad* mice. Consistent with PCREB up-regulation, BDNF protein expression was also higher in *gad* mice. Thus, excessive ubiquitin induction after ischemic injury may lead to the degradation of antiapoptotic proteins and suppression of the transcription of prosurvival proteins.[5–8,28]

Effect of UCH-L1 on Ischemia-Induced Neural Cell Apoptosis

To determine whether increased expression of antiapoptotic and prosurvival proteins in *gad* mice really leads to resistance against ischemia, we next examined the histology of ischemic retinas in both strains. As expected, ischemic damage in *gad* mice was mild compared with wild-type mice (Figure 3); the thickness of the inner retinal layer (IRL) (Figure 4A) and the percentage of surviving cells in the GCL (Figure 4B) after ischemia were significantly larger in *gad* mice. We also analyzed apoptotic cells in the retina by TUNEL staining. Control animals

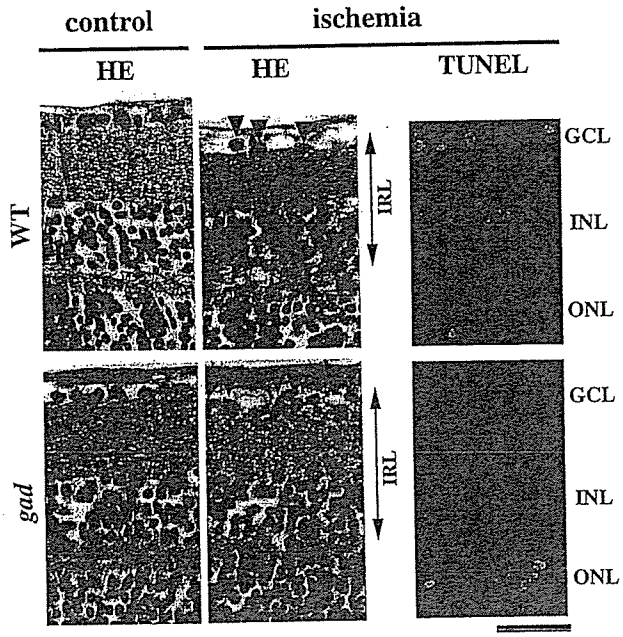

Figure 3. Representative pictures of HE staining (**left**) and TUNEL staining (**right**) in wild-type and *gad* mice retina before (control) and after ischemic injury (ischemia). Retinal damage 7 days after ischemia (HE staining) in *gad* mice was mild compared with wild-type mice. Consistently, TUNEL-positive cells 1 day after ischemia were observed only in the ONL in *gad* mice. Bar, 50 μm.

showed practically no signals in both strains (data not shown). However, in ischemic retinas, TUNEL-positive cells were observed in all three nuclear layers in wild-type mice, but mainly only in the outer nuclear layer (ONL) in *gad* mice (Figure 3). Consistently, quantitative analysis by ELISA demonstrated decreased retinal cell apoptosis in *gad* mice (Figure 4C). Ischemia-induced retinal cell apoptosis is executed by two distinct caspase proteases.

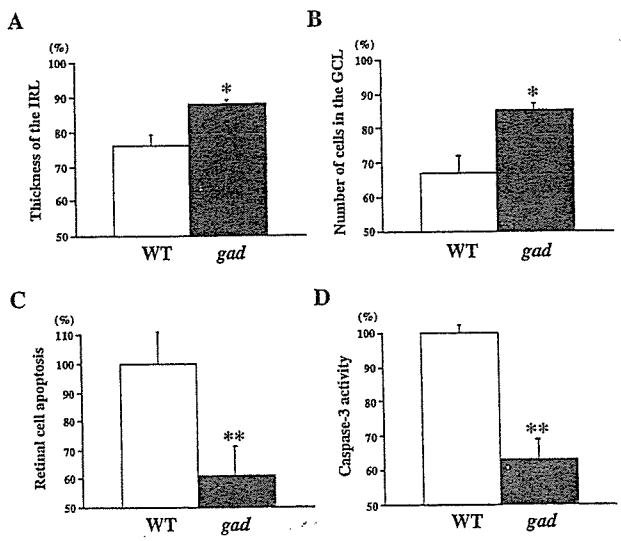

Figure 4. Effect of ischemic injury in wild-type and *gad* mice retina. Thickness of the IRL (arrows in Figure 3) (**A**) and the number of cells in the GCL (arrowheads in Figure 3) (**B**) in retina 7 days after ischemic injury as a percentage of the non-ischemic fellow eye. Quantitative analysis of retinal cell apoptosis (**C**) and caspase-3-like activity (**D**) in retina 1 day after ischemic injury. Results of six independent experiments are presented as mean ± SD (*, $P < 0.05$; **, $P < 0.01$).

Caspase-1 is predominantly associated with photoreceptor cell apoptosis in the ONL, whereas caspase-3 is more active in the GCL and INL for the same process.[29] To determine the mechanisms of strong tolerance against ischemia in *gad* mice, we next examined the activity of these two caspases in the ischemic retina. Caspase-1-like activity was not significantly different in *gad* mice compared with wild-type mice (80 ± 13%; P = not significant) (data not shown). On the other hand, caspase-3-like activity in *gad* mice was suppressed to 63 ± 6% compared with wild-type mice ($P < 0.01$) (Figure 4D).

Discussion

Ischemic injury is mainly associated with excessive concentrations of glutamate, which results in overactivation of glutamate receptors and initiates a cascade of events that leads to necrosis and/or apoptosis. Consistently, several studies have shown that retinal neurons can be protected by glutamate receptor antagonists.[17,30,31] An alternative strategy to attenuate glutamate neurotoxicity is keeping the extracellular glutamate concentration below neurotoxic levels. We previously demonstrated that selective inhibition of N-acetylated-α-linked-acidic dipeptidase (NAALADase), an enzyme responsible for the hydrolysis of neuropeptide N-acetyl-aspartyl-glutamate to N-acetyl-aspartate and glutamate, robustly protects neurons in a rat model of stroke[32] and in a mouse model of ischemic retinal injury.[17] Another possible target is the glutamate transporter.[33] There are four subtypes of glutamate transporters (GLAST, GLT-1, EAAC1, and EAAT5) in the retina.[16,33] By using GLAST and GLT-1 knockout mice,[34,35] we showed that both GLAST and GLT-1 (GLAST > GLT-1) are crucial for the protection of retinal cells from ischemic injury.[16]

In addition to these typical molecules involved in glutamate neurotoxicity, we first demonstrated that neuron-specific deubiquitinating enzyme, UCH-L1, is a new possible therapeutic target for ischemic retinal injury. In *gad* mice, functional loss of UCH-L1 results in the protection of retinal neurons following ischemic injury. One of the possible mechanisms is the accumulation of antiapoptotic proteins Bcl-2 and XIAP. Suppression of Bcl-2 leads to altered mitochondrial membrane permeability resulting in release of cytochrome c into the cytosol, which can trigger caspase activation leading to apoptosis.[23–26] On the other hand, a member of the IAP (inhibitor of apoptosis proteins) family, XIAP, can bind to and inhibit caspase-3 activation.[23–26] Consistently, retinal cell apoptosis in *gad* mice is suppressed mainly in the inner retina (Figure 3), where caspase-3 is more active than caspase-1.[27] These results suggest a possibility that functional loss of UCH-L1 may lead to decreased cytochrome c release from mitochondria and subsequent caspase inactivation in *gad* mice. If UCH-L1 inhibition works on the apoptotic pathway both before and after cytochrome c release from mitochondria,[23–26] this method may have a broader effect compared with the overexpression or suppression of a single antiapoptotic or apoptotic factor, respectively.

On the other hand, BDNF and PCREB protein expression levels were also up-regulated in *gad* mice. Recent studies have shown that trophic factors such as BDNF, ciliary neurotrophic factor (CNTF), basic fibroblast growth factor (bFGF), or glial cell line-derived neurotrophic factor (GDNF) increase RGC survival and regeneration.[36–45] Since CREB plays a central role in mediating responses of trophic factors including BDNF,[27] enhanced release of these trophic factors in *gad* mice may prevent ischemia-induced retinal cell apoptosis. We previously showed that, in addition to direct neuroprotection, these factors can alter secondary trophic factor production in retina-specific Müller glial cells, which indirectly regulate neural cell survival.[18,46] Consistently, intraocular injection of trophic factors induces the phosphorylated form of extracellular receptor kinase (pERK) or c-fos mainly in Müller cells.[47,48] Thus, loss of UCH-L1 may induce neural cell survival by stimulating both neural and glial cells.[18,46,49]

Ischemic retinal injury is implicated in a number of pathological states, such as retinal artery occlusion, glaucoma, and diabetic retinopathy.[16,17,30,31] Accordingly, the present results raise intriguing possibilities for the management of these pathological conditions by modifying the expression of UCH-L1 and activity of the ubiquitin-proteasome pathway.[50] Using this strategy with trophic factors,[18,46] NAALADase inhibitor,[17] glutamate transporter activators, such as bromocryptine,[51,52] or overexpression of GLAST or GLT-1,[16] may induce synergic effects on multiple cellular targets to prevent ischemia-induced neural cell apoptosis. However, due to the central function of the ubiquitin system in many basic cellular processes, modulation of this system can become a "double-edged sword".[1] Depletion of the free ubiquitin pool may cause accumulation of proteins that should be subjected to ubiquitin-dependent proteolysis. To address these critical issues, further investigations revealing the functional site of UCH-L1 and its involvement in ubiquitin induction *in vivo* will be needed.

Acknowledgments

We thank H.-M. A. Quah and L.F. Parada for critical reading of the manuscript, and members of the Wada lab for helpful discussions.

References

1. Hershko A, Ciechanover A, Varshavsky A: The ubiquitin system. Nat Med 2000, 6:1073–1081
2. DiAntonio A, Haghighi AP, Portman SL, Lee JD, Amaranto AM, Goodman CS: Ubiquitination-dependent mechanisms regulate synaptic growth and function. Nature 2001, 412:449–452
3. Finley D, Ozkaynak E, Varshavsky A: The yeast polyubiquitin gene is essential for resistance to high temperatures, starvation, and other stresses. Cell 1987, 48:1035–1046
4. Bond U, Agell N, Haas AL, Redman K, Schlesinger MJ: Ubiquitin in stressed chicken embryo fibroblasts. J Biol Chem 1988, 263:2384–2388
5. Dimmeler S, Breitschopf K, Haendeler J, Zeiher AM: Dephosphorylation targets Bcl-2 for ubiquitin-dependent degradation: a link between the apoptosome and the proteasome pathway. J Exp Med 1999, 189:1815–1822
6. Breitschopf K, Haendeler J, Malchow P, Zeiher AM, Dimmeler S: Posttranslational modification of Bcl-2 facilitates its proteasome-dependent degradation: molecular characterization of the involved signaling pathway. Mol Cell Biol 2000, 20:1886–1896
7. Daino H, Matsumura I, Takada K, Odajima J, Tanaka H, Ueda S, Shibayama H, Ikeda H, Hibi M, Machii T, Hirano T, Kanakura Y: Induction of apoptosis by extracellular ubiquitin in human hematopoietic cells: possible involvement of STAT3 degradation by proteasome pathway in interleukin 6-dependent hematopoietic cells. Blood 2000, 95:2577–2585
8. Yang Y, Fang S, Jensen JP, Weissman AM, Ashwell JD: Ubiquitin protein ligase activity of IAPs and their degradation in proteasomes in response to apoptotic stimuli. Science 2000, 288:874–877
9. Wilkinson KD, Lee KM, Deshpande S, Duerksen-Hughes P, Boss JM, Pohl J: The neuron-specific protein PGP 9.5 is a ubiquitin carboxyl-terminal hydrolase. Science 1989, 246:670–673
10. Wilkinson KD, Deshpande S, Larsen CN: Comparisons of neuronal (PGP 9.5) and non-neuronal ubiquitin C-terminal hydrolases. Biochem Soc Trans 1992, 20:631–637
11. Osaka H, Wang YL, Takada K, Takizawa S, Setsuie R, Li H, Sato Y, Nishikawa K, Sun YJ, Sakurai M, Harada T, Hara Y, Kimura I, Chiba S, Namikawa K, Kiyama H, Noda M, Aoki S, Wada K: Ubiquitin carboxy-terminal hydrolase L1 binds to and stabilizes monoubiquitin in neuron. Hum Mol Genet 2003, 12:1945–1958
12. Lowe J, McDermott H, Landon M, Mayer RJ, Wilkinson KD: Ubiquitin carboxyl-terminal hydrolase (PGP 9.5) is selectively present in ubiquitinated inclusion bodies characteristic of human neurodegenerative diseases. J Pathol 1990, 161:153–160
13. Leroy E, Boyer R, Auburger G, Leube B, Ulm G, Mezey E, Harta G, Brownstein MJ, Jonnalagada S, Chernova T, Dehejia A, Lavedan C, Gasser T, Steinbach PJ, Wilkinson KD, Polymeropoulos MH: The ubiquitin pathway in Parkinson's disease. Nature 1998, 395:451–452
14. Saigoh K, Wang YL, Suh JG, Yamanishi T, Sakai Y, Kiyosawa H, Harada T, Ichihara N, Wakana S, Kikuchi T, Wada K: Intragenic deletion in the gene encoding ubiquitin carboxy-terminal hydrolase in gad mice. Nat Genet 1999, 23:47–51
15. Harada T, Imaki J, Hagiwara M, Ohki K, Takamura M, Ohashi T, Matsuda H, Yoshida K: Phosphorylation of CREB in rat retinal cells after focal retinal injury. Exp Eye Res 1995, 61:769–772
16. Harada T, Harada C, Watanabe M, Inoue Y, Sakagawa T, Nakayama N, Sasaki S, Okuyama S, Watase K, Wada K, Tanaka K: Functions of the two glutamate transporters GLAST and GLT-1 in the retina. Proc Natl Acad Sci USA 1998, 95:4663–4666
17. Harada C, Harada T, Slusher BS, Yoshida K, Matsuda H, Wada K: N-acetylated-α-linked-acidic dipeptidase inhibitor has a neuroprotective effect on mouse retinal ganglion cells after pressure-induced ischemia. Neurosci Lett 2000, 292:134–136
18. Harada T, Harada C, Nakayama N, Okuyama S, Yoshida K, Kohsaka S, Matsuda H, Wada K: Modification of glial-neuronal cell interactions prevents photoreceptor apoptosis during light-induced retinal degeneration. Neuron 2000, 26:533–541
19. Yamazaki K, Wakasugi N, Tomita T, Kikuchi T, Mukoyama M, Ando K: Gracile axonal dystrophy (GAD), a new neurological mutant in the mouse. Proc Soc Exp Biol Med 1988, 187:209–215
20. Naash MI, Al-Ubaidi MR, Anderson RE: Light exposure induces ubiquitin conjugation and degradation activities in the rat retina. Invest Ophthalmol Vis Sci 1997, 38:2344–2354
21. Bonfoco E, Krainc D, Ankarcrona M, Nicotera P, Lipton SA: Apoptosis and necrosis: two distinct events induced, respectively, by mild and intense insults with N-methyl-D-aspartate or nitric oxide/superoxide in cortical cell cultures. Proc Natl Acad Sci USA 1995, 92:7162–7166
22. Szabo ME, Haines D, Garay E, Chiavaroli C, Farine JC, Hannaert P, Berta A, Garay RP: Antioxidant properties of calcium dobesilate in ischemic/reperfused diabetic rat retina. Eur J Pharmacol 2001, 428:277–286
23. Tsujimoto Y, Shimizu S: Bcl-2 family: life-or-death switch. FEBS Lett 2000, 466:6–10
24. Ranger AM, Malynn BA, Korsmeyer SJ: Mouse models of cell death. Nat Genet 2001, 28:113–118
25. Deveraux QL, Reed JC: IAP family proteins: suppressors of apoptosis. Genes Dev 1999, 13:239–252
26. Green DR: Apoptotic pathways: paper wraps stone blunts scissors. Cell 2000, 102:1–4

27. Finkbeiner S: CREB couples neurotrophin signals to survival messages. Neuron 2000, 25:11–14
28. Taylor CT, Furuta GT, Synnestvedt K, Colgan SP: Phosphorylation-dependent targeting of cAMP response element binding protein to the ubiquitin/proteasome pathway in hypoxia. Proc Natl Acad Sci USA 2000, 97:12091–12096
29. Katai N, Yoshimura N: Apoptotic retinal neuronal death by ischemia-reperfusion is executed by two distinct caspase family proteases. Invest Ophthalmol Vis Sci 1999, 40:2697–2705
30. Lipton SA: Retinal ganglion cells, glaucoma and neuroprotection. Prog Brain Res 2001, 131:712–718
31. Osborne NN, Melena J, Chidlow G, Wood JP: A hypothesis to explain ganglion cell death caused by vascular insults at the optic nerve head: possible implication for the treatment of glaucoma. Br J Ophthalmol 2001, 85:1252–1259
32. Slusher BS, Vornov JJ, Thomas AG, Hurn PD, Harukuni I, Bhardwaj A, Traystman RJ, Robinson MB, Britton P, Lu XC, Tortella FC, Wozniak KM, Yudkoff M, Potter BM, Jackson PF: Selective inhibition of NAALADase, which converts NAAG to glutamate, reduces ischemic brain injury. Nat Med 1999, 5:1396–1402
33. Tanaka K: Functions of glutamate transporters in the brain. Neurosci Res 2000, 37:15–19
34. Tanaka K, Watase K, Manabe T, Yamada K, Watanabe M, Takahashi K, Iwama H, Nishikawa T, Ichihara N, Kikuchi T, Okuyama S, Kawashima N, Hori S, Takimoto M, Wada K: Epilepsy and exacerbation of brain injury in mice lacking the glutamate transporter GLT-1. Science 1997, 276:1699–1702
35. Watase K, Hashimoto K, Kano M, Yamada K, Watanabe M, Inoue Y, Okuyama S, Sakagawa T, Ogawa S, Kawashima N, Hori S, Takimoto M, Wada K, Tanaka K: Motor discoordination and increased susceptibility to cerebellar injury in GLAST mutant mice. Eur J Neurosci 1998, 10:976–988
36. Mey J, Thanos S: Intravitreal injections of neurotrophic factors support the survival of axotomized retinal ganglion cells in adult rats in vivo. Brain Res 1993, 602:304–317
37. Cohen A, Bray GM, Aguayo AJ: Neurotrophin-4/5 (NT-4/5) increases adult rat retinal ganglion cell survival and neurite outgrowth in vitro. J Neurobiol 1994, 25:953–959
38. Mansour-Robaey S, Clarke DB, Wang YC, Bray GM, Aguayo AJ: Effects of ocular injury and administration of brain-derived neurotrophic factor on survival and regrowth of axotomized retinal ganglion cells. Proc Natl Acad Sci USA 1994, 91:1632–1636
39. Unoki K, LaVail MM: Protection of the rat retina from ischemic injury by brain-derived neurotrophic factor, ciliary neurotrophic factor, and basic fibroblast growth factor. Invest Ophthalmol Vis Sci 1994, 35: 907–915
40. Hammes HP, Federoff HJ, Brownlee M: Nerve growth factor prevents both neuroretinal programmed cell death and capillary pathology in experimental diabetes. Mol Med 1995, 1:527–534
41. Bosco A, Linden R: BDNF and NT-4 differentially modulate neurite outgrowth in developing retinal ganglion cells. J Neurosci Res 1999, 57:759–769
42. Yan Q, Wang J, Matheson CR, Urich JL: Glial cell line-derived neurotrophic factor (GDNF) promotes the survival of axotomized retinal ganglion cells in adult rats: comparison to and combination with brain-derived neurotrophic factor (BDNF). J Neurobiol 1999, 38:382–390
43. Di Polo A, Aigner LJ, Dunn RJ, Bray GM, Aguayo AJ: Prolonged delivery of brain-derived neurotrophic factor by adenovirus-infected Müller cells temporarily rescues injured retinal ganglion cells. Proc Natl Acad Sci USA 1998, 95:3978–3983
44. Koeberle PD, Ball AK: Neurturin enhances the survival of axotomized retinal ganglion cells in vivo: combined effects with glial cell line-derived neurotrophic factor and brain-derived neurotrophic factor. Neuroscience 2002, 110:555–567
45. Peterson WM, Wang Q, Tzekova R, Wiegand SJ: Ciliary neurotrophic factor and stress stimuli activate the Jak-STAT pathway in retinal neurons and glia. J Neurosci 2000, 20:4081–4090
46. Harada T, Harada C, Kohsaka S, Wada E, Yoshida K, Ohno S, Mamada H, Tanaka K, Parada LF, Wada K: Microglia-Müller glia cell interactions control neurotrophic factor production during light-induced retinal degeneration. J Neurosci 2002, 22:9228–9236
47. Wahlin KJ, Campochiaro PA, Zack DJ, Adler R: Neurotrophic factors cause activation of intracellular signaling pathways in Müller cells and other cells of the inner retina, but not photoreceptors. Invest Ophthalmol Vis Sci 2000, 41:927–936
48. Wahlin KJ, Adler R, Zack DJ, Campochiaro PA: Neurotrophic signaling in normal and degenerating rodent retinas. Exp Eye Res 2001, 73:693–701
49. Bringmann A, Reichenbach A: Role of Müller cells in retinal degenerations. Front Biosci 2001, 6:E72–E92
50. Nishikawa K, Li H, Kawamura R, Osaka H, Wang YL, Hara Y, Hirokawa T, Manago Y, Amano T, Noda M, Aoki S, Wada K: Alterations of structure and hydrolase activity of parkinsonism-associated human ubiquitin carboxyl-terminal hydrolase L1 variants. Biochem Biophys Res Commun 2003, 304:176–183
51. Yamashita H, Kawakami H, Zhang YX, Tanaka K, Nakamura S: Neuroprotective mechanism of bromocriptine. Lancet 1995, 346:1305
52. Yamashita H, Kawakami H, Zhang YX, Tanaka K, Nakamura S: Effect of amino acid ergot alkaloids on glutamate transport via human glutamate transporter hGluT-1. J Neurol Sci 1998, 155:31–36

Microbiol. Immunol., 48(12), 985–994, 2004

Editor-Communicated Paper

Quantum Dots Targeted to the Assigned Organelle in Living Cells

Akiyoshi Hoshino[1,2,3], Kouki Fujioka[1], Taisuke Oku[1,4], Shun Nakamura[5], Masakazu Suga[1], Yukio Yamaguchi[4], Kazuo Suzuki[3], Masato Yasuhara[2], and Kenji Yamamoto*[,1,2]

[1]*Department of Medical Ecology and Informatics, Research Institute, International Medical Center of Japan, Shinjuku-ku, Tokyo 162–8655, Japan,* [2]*Department of Pharmacokinetics and Pharmacodynamics, Hospital Pharmacy, Tokyo Medical and Dental University, Bunkyo-ku, Tokyo 113–8519, Japan,* [3]*Department of Bioactive Molecules, National Institute of Infectious Diseases, Shinjuku-ku, Tokyo 162–8640, Japan,* [4]*Department of Chemical System Engineering, School of Engineering, University of Tokyo, Bunkyo-ku, Tokyo 113–8656, Japan, and* [5]*Division of Biochemistry and Cellular Biology, National Institute of Neuroscience, Kodaira, Tokyo 187–8502, Japan*

Communicated by Dr. Hidechika Okada: Received October 8, 2004. Accepted October 21, 2004

Abstract: **Fluorescent nanocrystal quantum dots (QDs) have the potential to be applied to bioimaging since QDs emit higher and far longer fluorescence than conventional organic probes. Here we show that QDs conjugated with signal peptide obey the order to transport the assigned organelle in living cells. We designed the supermolecule of luminescent QDs conjugated with nuclear- and mitochondria-targeting ligands. When QDs with nuclear-localizing signal peptides were added to the culture media, we can visualize the movements of the QDs being delivered into the nuclear compartment of the cells with 15 min incubation. In addition, mitochondrial signal peptide can also transport QDs to the mitochondria in living cells. In conclusion, these techniques have the possibility that QDs can reveal the transduction of proteins and peptides into specific subcellular compartments as a powerful tool for studying intracellular analysis *in vitro* and even *in vivo*.**

Key words: **Quantum dot, Signal peptide, Nanocrystal, Nuclear localizing signal, Mitochondria targeting signal, Bioimaging**

Nanotechnology is the technology of designing, manufacturing, and utilizing the "supermolecule materials" which have the specific function based on their nanometer size. The "supermolecule" said here is a functional unit of two meanings; (1) A supermolecule consists of each molecule that has a certain mutual interaction and relation with one another, (2) A supermolecule shows its specific function as a whole molecule. Ultrafine nanocrystals have been expected to be applied widely in biomedical fields as biomaterials, immunoassay, diagnostics, and even in therapeutics (7, 9, 18, 32, 34, 40, 41). One of them, nanocrystal quantum dots (QDs), is widely used as stable and bright fluorophores that can have high quantum yields, narrow luminescent spectra, high absorbency, high resistance to photobleaching, and can provide excitation of several different emission colors using a single wavelength for excitation (4, 19).

In the field of molecular biology, fluorescent tagging of cells and biomolecules with organic fluorophores such as FITC has been used for a long time for these purposes of tracking biomolecules. But unfortunately, the use of organic fluorophores for living-cell applications is subject to certain limitations, because most of fluorophores photobleach easily (17). These organic fluorophores have their broad emission bands, which limit the number of fluorescent probes that can be simultaneously resolved. In addition, there are a lot of bright fluorophores, such as Hoechst® dyes and a rhodamine 123 derivative (Mitotracker®) (20), used for stain of nuclei and mitochondria, but these fluorophores cannot transport proteins or other molecules to the target

**Address correspondence to* Dr. Kenji Yamamoto, Department of Medical Ecology and Informatics, Research Institute, International Medical Center of Japan, Toyama 1–21–1, Shinjuku-ku, Tokyo 162–8655, Japan. Fax: +81–3–3202–7364. E-mail: backen@ri.imcj.go.jp

Abbreviations: MPA, 3-mercaptopropanoic acid; QD, quantum dot; TOPO, *n*-trioctylphosphine oxide.

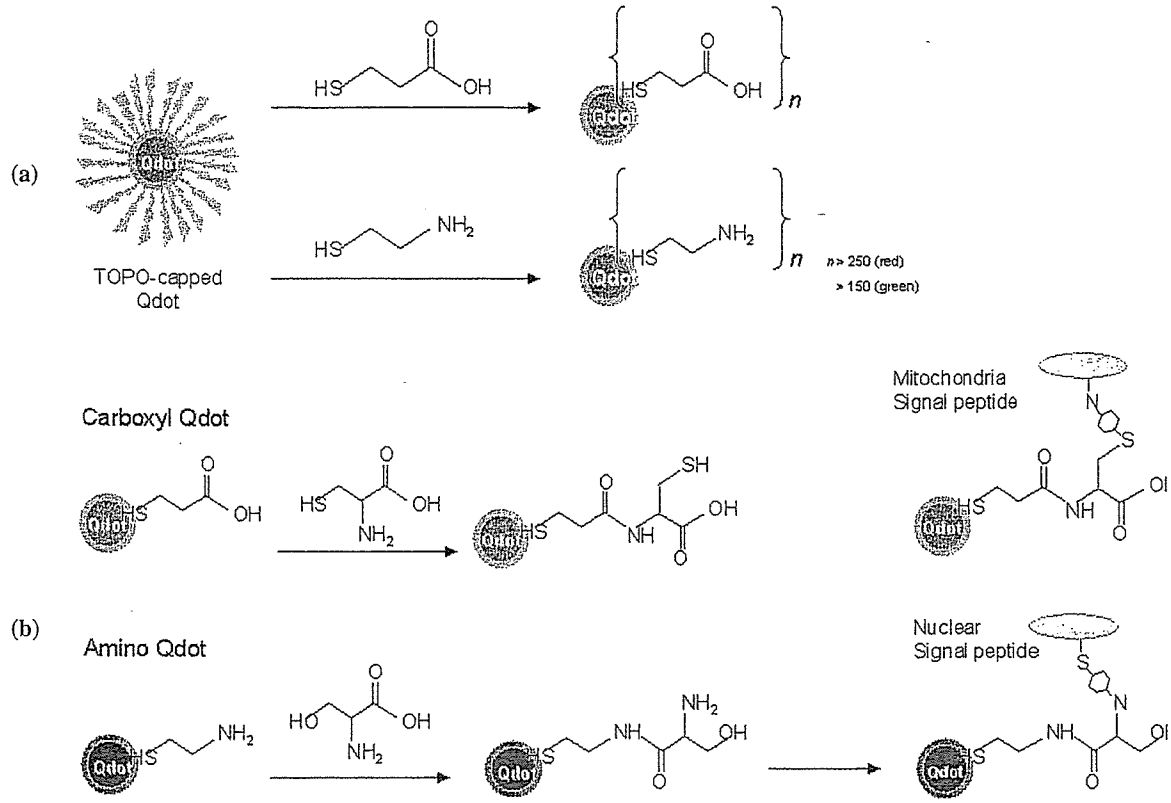

Fig. 1. Schematic illustration of peptide conjugated QDs for organelle targeting and imaging. (a) Chemically synthesized TOPO-capped QDs were replaced by MPA or cysteamine using thiol-exchange reactions. After reaction, QDs were covered with approximately 250 carboxyl or amine groups per particle. (b) A two-step conjugation strategy of QD-oligopeptide probes. MPA-QD (upper lane) or cysteamine-QD (lower lane) was primarily coupled with amine groups of cysteine or serine by using EDC coupling reagents. Then amino acid-coated QDs were secondarily conjugated with target peptides by coupling between *N*-hydroxysuccinimidyl and maleimide groups.

organelle. On the other hand, the signal peptides with organic fluorophore cannot trace the luminescent for long time observation. In contrast, QDs are stabilized over a far longer exposure-time to light and can emit fluorescence of higher luminosity than the conventional organic fluorescence probes (5, 8, 27). Therefore, QDs are suitable for designing the supermolecule that supplemented the biological effects to itself, and applications with QDs are now widely performed as long-time fluorescent markers for efficient collection of fluorescence (3, 17, 22, 24, 35).

Once our synthesized QDs were enfolded into the hydrophobic micelles and completely dissolved in aqueous solution, which promotes several innovations to improve the solubility to apply for biological methods (2, 10, 11, 23). The water-soluble QDs in our previous method have lower stability for low pH or salt-containing buffer (14). There is very little amount of conjugate by using these QDs, since the most of QDs were easily aggregated under the conditions that combine QD with peptides or protein. Therefore, we could only utilize QDs as the high fluorescence cell-tracking markers (14, 33). We previously reported that several novel surface-modified QDs using carboxylic acids, polyalcohols, or amines showed various physicochemical properties (16). In this article, we established a two-step conjugating method as shown in Fig. 1. The QDs of carboxyl groups were primarily coupled with amine groups of cysteine monomer, and QDs of amine groups were with carboxylic groups of serine monomer, respectively. The obtained amino acid-coated QDs, which were stable for the pH changes, were secondarily conjugated with target peptides/proteins by using their sulfhydryl and amine groups.

Some proteins and peptides have been demonstrated to penetrate through the plasma membrane of cells by their protein transduction domains (12, 21, 26, 31). Previous studies defined that protein transduction by nuclear localizing peptides was an efficient method to deliver proteins into the nuclei of cells (25, 37). In this study we tried to label two functional oligopeptides transported to nuclear localizing or mitochondria, and

evaluated whether QD-peptide complex worked as the specific functional supermolecule based on original peptides.

Materials and Methods

Synthesis of hydrophilic QDs. Synthesis of ZnS-coated CdSe nanocrystal QDs (fluorescence wavelength: approximately 642 nm emitted red, and approximately 518 nm emitted green), which were enfolded into the micelle of *n*-trioctylphosphine oxide (TOPO), was previously reported (6, 15). 3-Mercaptopropanoic acid (MPA) and 2-aminoethanethiol (cysteamine hydrochloride) were used to obtain two kinds of hydrophilic QDs (carboxyl- and amino-QDs) by thiol exchange methods. In the case of carboxyl-QD, 50 mg of TOPO-QDs were dissolved into 1 ml tetrahydrofuran (THF) in a 4 ml-volume flasket, and then 250 μl MPA (Sigma-Aldrich, St. Louis, Mo., U.S.A.) were added. Then the mixture was heated at 85 C for 24 hr. In the case of amino-QD, primarily 250 mg cysteamine (Wako Pure Chemicals, Tokyo) was heated at 85 C in a flask (16). After melting, 50 mg/ml TOPO-QDs in THF was dropped to the flask and heated at 85 C for 2 hr. After the reaction, the turbid solution was collected and centrifuged at maximum speed. After it dried up, purified water was added to the residue, and centrifuged at maximum speed to remove the insoluble residue. The supernatant fraction containing soluble QDs was collected. After purified by Sephadex G-25 column (Amersham Biosciences, Piscataway, N.J., U.S.A.), QDs were concentrated and powderized by vacuum distillation. QDs were reconstituted in purified water before use.

Preparation of peptide-conjugated QDs. Amino acid sequences of three well-known functional oligopeptides described below were chemically synthesized; nuclear localizing peptide (R_{11}KC, sequenced NH_2-RRRRRRRRRRRKC-COOH) (25), mitochondria targeting signal sequence of cytochrome-*c* oxidase VIII subunit (Mito-8, sequenced NH_2-MSVLTPLLLRGLTGSARRLPVPRAKIHWLC-COOH) (13) or control mitochondrial peptide (START, sequenced NH_2-STARTSTARTSTARTSC-COOH) (1). The peptides were conjugated to QDs by a two-step reaction. Initially, 100 μM QD solution was mixed with equal volume of 100 mM cysteine solution in coexistent with 100 mM EDC coupling reagents (Pierce Biotechnology, Rockford, Ill., U.S.A.) and continuously mixed at 4 C for 1 hr. After removed of free-amino acid by Nap-5 column (Amersham Biosciences), about 10-fold mol of target peptides were secondarily conjugated with QD by using sulfo-SMCC coupling reagents (Pierce Biotech) and sonicated for 2 hr at 4 C. Products were purified using ultra-filtration membrane (NMWL 10000, Centriprep® Millipore). Finally, purified QD-peptide conjugates were filtrated with 0.1-μm membrane filters (Millipore) before use. To analyze the protein content of QD-conjugated peptides, conjugated QDs was plated to 96-well microplate and RC-DC Protein Assay reagent (Bio-Rad, Hercules, Calif., U.S.A.) was added. Six hundred fifty nanometer absorbance was measured by microplate reader (Bio-Rad). MPA-coated QD without coupling with any peptides was used as negative control.

Assessment of QD-uptake by cells. Vero cells were cultured in DMEM/F12 supplemented with 5% heat-inactivated fetal bovine serum at 37 C. To avoid the non-specific binding of QDs on the glass, 10 mm glass-based culture dish (Matsunami Glass Industries, Japan) was pre-coated with poly-L-lysine (Peptide Institute Co., Ltd., Osaka, Japan). The cells were plated at a volume of 1×10^5 cells/well on a glass-based dish. Then cells were stimulated with the indicated concentration of QD-peptides. After incubation, the cells were washed with PBS 5 times to remove the non-specific binding QDs, and the cells were fixed, and embedded in the glycerol containing 0.1% sodium azide. In the case of co-localization assay, cells were observed with a confocal microscopy MRC-1024 (Bio-Rad). Time course of R_{11}KC-coated QDs was examined on the fluorescence microscopy system equipped with a CO_2 incubator (IM-310 cell-culture microscope system, Olympus, Japan). Images were acquired with a digital camera D1X (Nikon) under fluorescent microscopy IX-81 (Olympus) using WIR mirror unit to adjust excitation wavelength over 610 nm.

Results and Discussion

Some oligopeptides have been demonstrated to penetrate across the cellular membrane by their protein transduction domains and specifically located to their designated organelle (12, 21, 26, 31). Previous studies showed that the protein transduction by nuclear localizing signal oligopeptide was an efficient method of delivering proteins into the nuclei of cells (37). To establish the supermolecule design that supplemented the biological effects to nanocrystal, we conjugated two kinds of functional NLS and MTS oligopeptides, which were transported to nuclear or mitochondria (13, 25). Then we evaluated that QD-peptide complex worked as the specific supermolecule those functions were based on their original peptides.

For the achievements of assemble QD-supermolecule, we established a two-step conjugating method as shown in Fig. 1. Briefly, QDs were coupled with amino

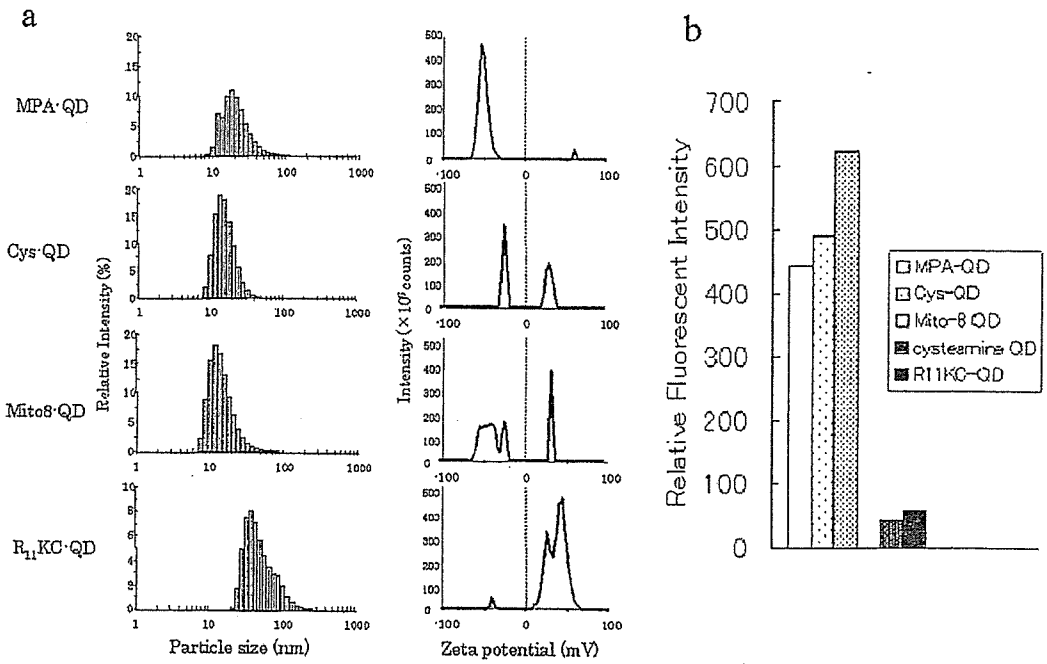

Fig. 2. Physicochemical properties of oligopeptide-conjugated QDs. (a) Particle size distribution of various QDs in aqueous solution (left) was measured by dynamic light scattering methods. Values are the mean±standard deviation of the data measured 12 times, respectively. Surface ζ-potential of QDs (right) was measured by electrophoresis. The line shows the electrophoretic mobility of these QDs in the stationary layers of 30 assays. Data shows the average of 30 assays. (b) Relative fluorescence intensity of QDs solution (10 μM) were measured by fluorospectrometer. QDs were excited by 365 nm wavelength (UV-A) and luminescence intensity of peak emission wavelength (519 nm) was detected.

acid at the first step, and secondarily coupled with the target oligopeptide. We prepare two kinds of QD whose surfaces were covered with carboxyl and sulfhydryl, and with NH_2 and hydroxyl groups, respectively. MPA-QDs were primarily coupled with amine groups of cysteine by using EDC coupling reagents (cys-QD). In the case of amine-QDs, they were also coupled with carboxylic groups of serine (ser-QD). The surface of the obtained QD was covered with approximately 450 amino acids per particle (data not shown). Both of the newly obtained amino acid-coated QDs, which were stable for changes of pH, were secondarily conjugated with target peptides by coupling with their sulfhydryl and amine groups by sulfo-SMCC reagents. In this study, we conjugated two kinds of signaling peptide; nuclear localizing signal (NLS) oligopeptide $R_{11}KC$ (25), and mitochondria targeting signal (MTS) oligopeptide Mito-8 (13). Mito-8 peptides were coupled with cys-QDs, and basic $R_{11}KC$-peptides were with ser-QDs, respectively. The number of peptide with QDs were calculated based on RC-DC protein assay, indicating that QD-$R_{11}KC$ and QD-Mito-8 were covered with 48 and 62 peptides per particle, respectively (data not shown). To assess the change of physicochemical properties of QDs after conjugated with oligopeptides, the particle size and surface potential of peptide-conjugated QDs were observed by a dynamic light scattering method. This surface potential of QDs was drastically changed after conjugated with peptides (Fig. 2a). In this labeling method, the average of the observed particle size distribution tends to increase, because it is hardly avoidable to control the excess polymerization. Previously, we tried to target signal peptides directly to MPA-QDs, resulted in aggregation, especially in the case of amine-rich oligopeptides because of salt-formation between carboxylic groups of QD and amine groups of target peptides (16). This novel two-step method enables to QDs labeled even in amine-rich basic oligopeptides such as $R_{11}KC$. Our previous study demonstrated that the fluorescence intensity of QD was also dramatically changed by the surface-covered molecules of QD particle (16, 22). We previously tried to cover QDs directly with cysteine monomer, which resulted in losing luminescence during the labeling process, because of electron leakage through the surface NH_2 group (16). Therefore, we assessed whether the fluorescent intensity of QDs changed or diminished during the peptide coupling process. After the first reaction step, slight change of luminescent intensity was observed. But the fluores-

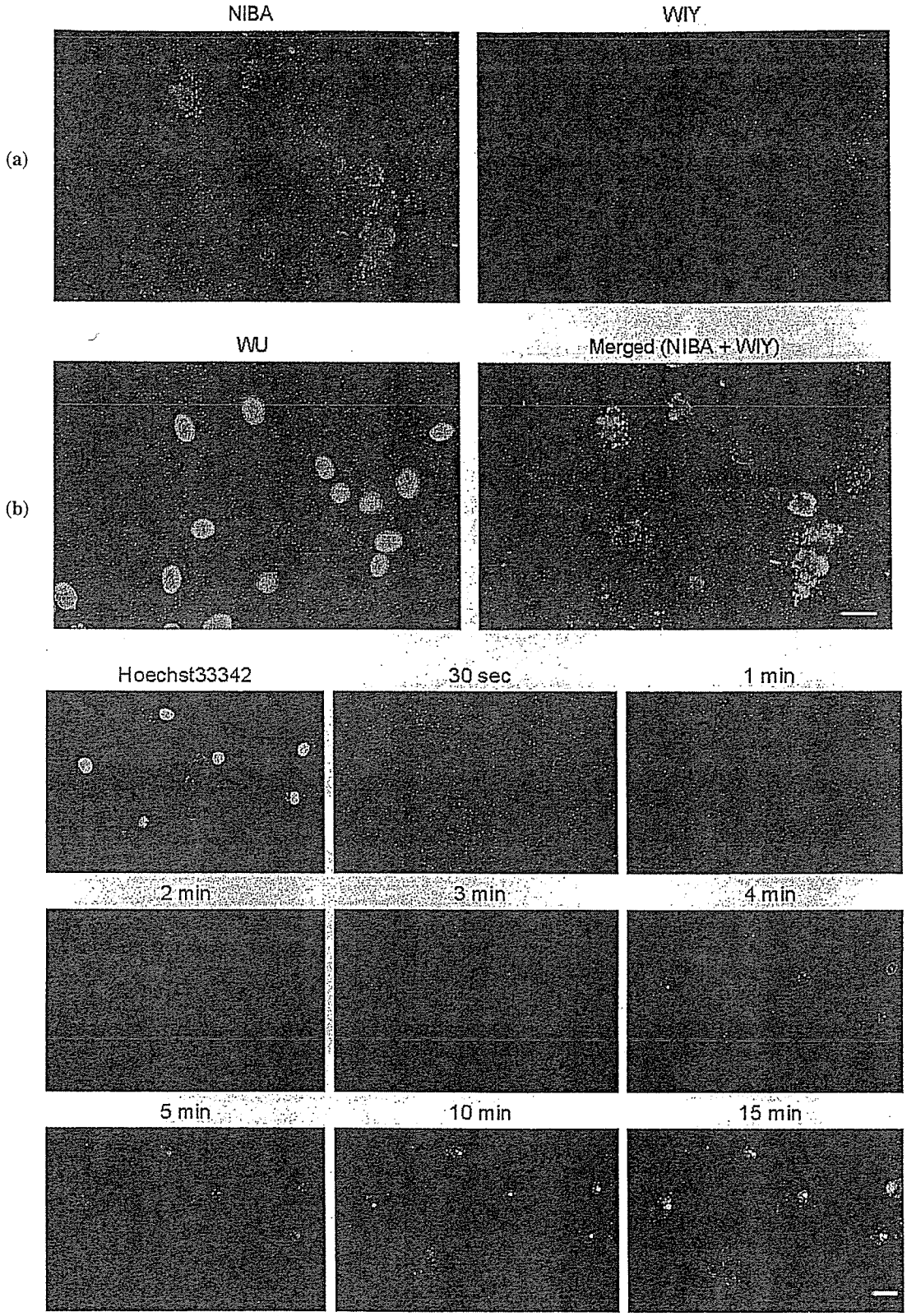

Fig. 3. Localization of R_{11}KC-conjugated QDs to nucleus. (a) Cells were pre-stained with Hoechst®33342, and stimulated with FITC-labeled QD-conjugated R_{11}KC peptide (1 μM final) for 3 hr at 37 C with 5% CO_2 condition. (b) Cells were pre-stained with Hoechst®33342, and stimulated with QD-R^{11}KC (1 μM final) for the indicated time at 37 C under 5% CO_2 condition with a culture fluorescence microscope (IM-310 system, Olympus). Images were taken using D1X digital camera (Nikon) equipped with IM-310 system at the indicated time by a 3 sec exposure. Bars indicated 10 μm.

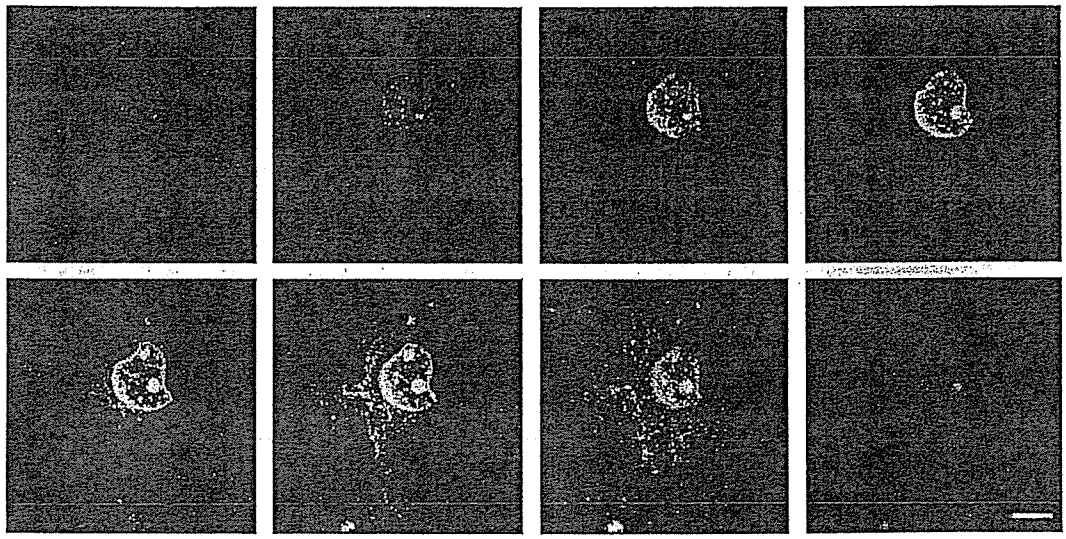

Fig. 4. R_{11}KC-conjugated QDs were accumulated in nucleous. Cells were stimulated by R_{11}KC-QD as described in Fig. 3. The cells were observed by confocal microscopy. The images are collected in the Z-direction at the span of 0.1 μm. Bars indicated 10 μm. Magnifications: ×120.

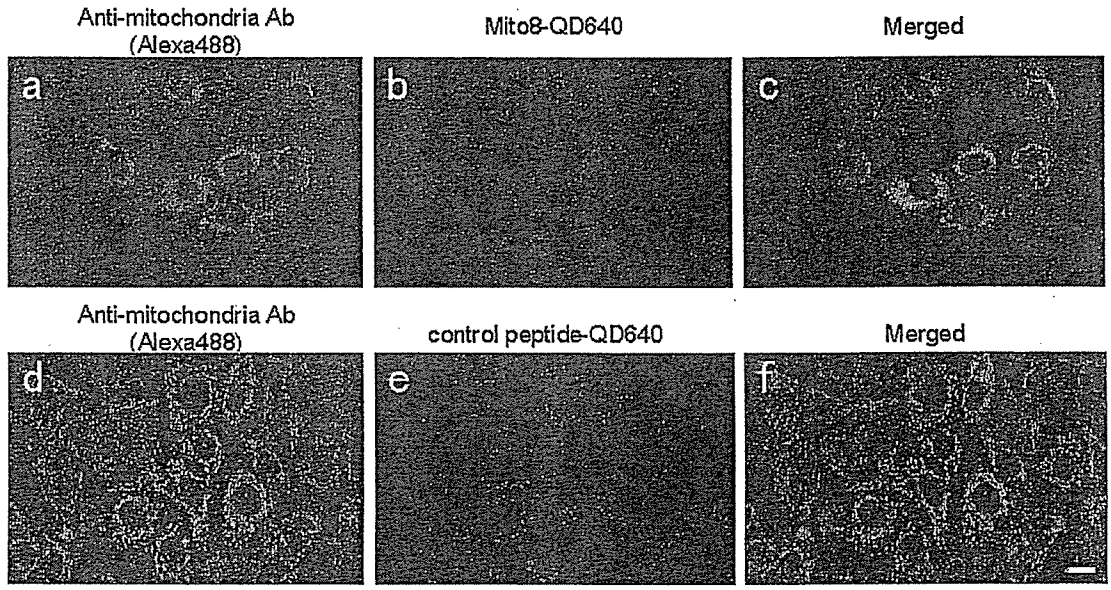

Fig. 5. Mitochondria images of Vero cells. Vero cells were stimulated with 1 μM with Mito-8 QD640 (a–c) or control START QD640 (d–f), and incubated for 12 hr under 37 C conditions. Cells were then fixed, and stained with anti-human mitochondria (M2) antibody. The cells were observed by fluorescent microscopy. Bars indicated 10 μm.

cence intensity enhanced remarkably after the secondary coupling with the target peptide (Fig. 2b). This result suggested that covering QD with the high molecular weight polymer such as polypeptides might prohibit the leakage of electron and might contribute to the continuative electron-rich condition of whole QD particle.

Next we evaluated whether the function of signal peptides would be held after conjugated with QDs. To confirm this, FITC-conjugated R_{11}KC peptides were conjugated with QD640 (fluorescence 640 nm, emitted red) and added to the cultured COS7 cells. We previously reported that QD without any peptides resulted in cellular-uptake into endosome by endocytotic pathways (17, 33). In this case, the red fluorescence from QD was located in nucleus and co-localized with that from FITC (Fig. 3a). This result indicated that QDs with nuclear peptides acquire another function that was based on R_{11}KC peptides. Unlabeled R_{11}KC remained in this study because the labeling efficiency of QDs with

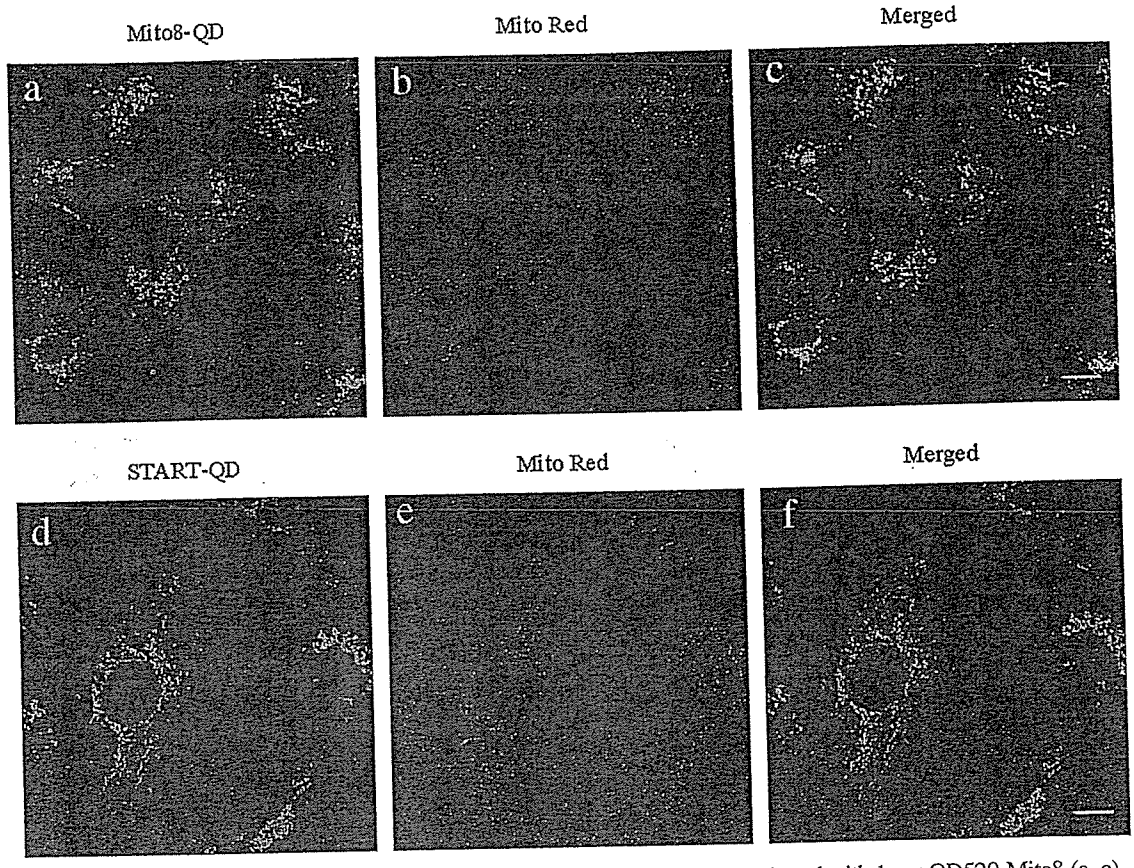

Fig. 6. Living mitochondria images by confocal microscope. Vero cells were cultured with 1 μM QD520-Mito8 (a–c) or QD520-START (control peptide, d–f) for 12 hr under 37 C conditions. Then cells were co-stimulated with MitoRed® mitochondria staining reagents (Dojindo Laboratories) for more additional 1 hr. After stimulation, cells were observed by confocal microscopy as shown in Fig. 4. Bars indicated 20 μm. Magnifications: ×80.

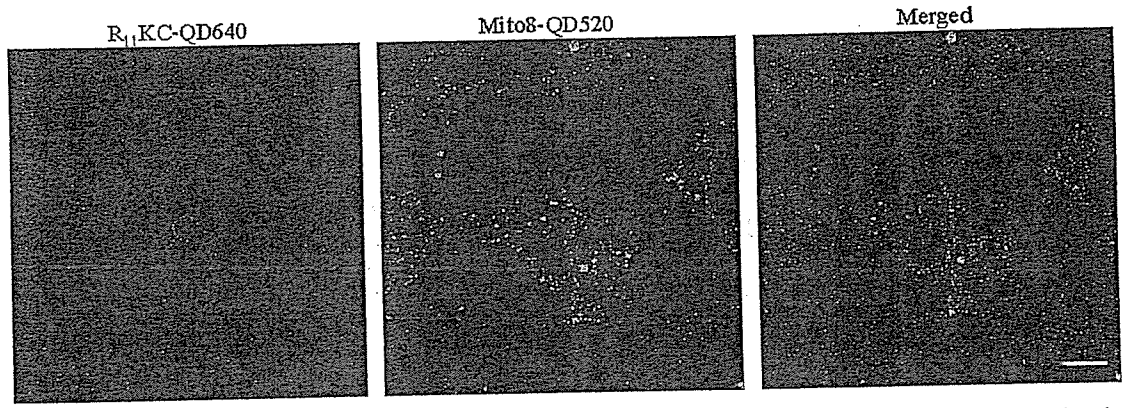

Fig. 7. Two kinds of signal peptide-QD showed independent behavior in the cells. Vero cells were co-stimulated with 1 μM QD640-Mito8 (emitted red) and QD-R_{11}KC (emitted green) for 12 hr under 37 C conditions. After fixed, the cells were observed by confocal microscopy. Bars indicated 20 μm.

oligopeptides was approximately 40% in this method and almost all of the FITC-tagged R_{11}KCs were not labeled with QDs. This result indicated that the R_{11}KC-QD has the same capability to localize into a nucleus as original ones. It is already reported that R_{11}KC peptide is rapidly localized into a nucleus by incubating for 10 min (25, 39). Then we tried to track the footmark of R_{11}KC peptide into nucleus in living cells for 15 min. Vero cells were treated with R_{11}KC-conjugated QD640 and continuously observed under a culture fluorescent microscopy (Fig. 3b). The penetration from the cell membrane to nuclei was observed about 30 sec after incubation, and precedently located into nucleus after 1 min. R_{11}KC-QDs were gradually accumulated the

whole nucleus during 15 min incubation. To investigate the localization of R_{11}KC-QDs into the nucleus, QDs distribution in the nucleus was observed by confocal microscopy (Fig. 4). R_{11}KC-QDs were dispersed in the whole nucleus and partially accumulated in nucleolus. In this study, we demonstrated that QDs as well as other fusion protein could also transit into nucleus with the help of nuclear signaling peptides.

Next we assessed the function of mitochondria signal peptides with QDs (Fig. 5). Mito-8 peptide- and control START peptide-coated QD640 (fluorescence 640 nm, emitted red) were incubated with cells and stained with anti-mitochondrial antibody. QD-red signal with Mito-8 gave raise to yellow in merged images (Fig. 5c). In contrast, red fluorescence emitted from control START peptides was not co-localized with that of mitochondria signal (Fig. 5f). Then we tried to visualize mitochondria distribution in living cells. Mito8-QD520 peptide was co-cultured with MitoRed® mitochondria staining dyes (Dojindo Laboratories, Japan). After incubation, the cells were observed by confocal laser microscopy (Fig. 6). QD-Mito-8 green luminescences from QD520 were also co-localized with conventional mitochondria probes. These results indicated that QDs with functional oligopeptides possessed dual functions to localize specific organelle and to emit high detectable fluorescence. Then we demonstrate the mixture of those two peptide separately move to their assigned organelle. The mixture of R_{11}KC-QD640 and Mito-8-QD520 were added to the Vero cells (Fig. 7). Red luminescence from R_{11}KC was separated from green ones from Mito-8 and not co-localized with each other, implying that QDs with functional peptides were individually transported to the target organelle.

Now several groups have reported that QDs conjugated with antibodies and some peptides for biological assays and cellular imaging *in vitro* and *in vivo* were demonstrated as brighter and longer lifetime probes (27–30). In this article, we demonstrated the various signal peptides conjugated with fluorescent QDs to both deliver QDs into living cells and selectively target specific organelles in living cells. In addition, these peptides-QD complexes have ability to translocate itself across the cell plasma membrane and can subsequently home to their specific targets such as the nucleus or the mitochondria. These results indicated that we succeeded in adding the new function as "information" to QDs by conjugating them with peptides. Our previous studies showed that QD-conjugated albumin and QD-glycerol can be targeted to the endosome and cytoplasm, respectively (14, 17). We showed in this article that QDs with targeted peptides can be also transported to nuclei and mitochondria. These techniques have the possibility that QDs can reveal transduction of proteins and peptides to specific subcellular compartments *in vitro* and even *in vivo* as a powerful tool for conducting intracellular analysis. We suggest that this technology could have a significant impact on the field of molecular and cellular biology as well as biotechnology. Recently, the plan that applied a novel nanomaterial such as nanocrystal QDs to the medical field attracted attention as one of the industrial applications of nanotechnology. And what is more, it is expected that QDs will be applied in the medical field for the innovative investigation, diagnosis and treatment of various diseases (8, 36, 38). It is very important to produce nanometer-sized materials with biological function, since we have no "designed material" which can arbitrarily penetrate nanometer-size gaps such as the skin, membrane, a blood vessel, and so on. This study demonstrates that these surface modifications of functional molecules combined with nanoparticles may work as bio-nanomachines conforming to the functions designated by their surface molecules. Nanomaterials have a great capacity of changing even the concept of existing diagnosis and medical treatment, by giving functions such as the pharmacological and magnetic effects, by giving the information of the specificity to tissue or organs *in vivo*. Novel nanomaterials including QD-supermolecules can be utilized as a transporter of the intracellular drug and gene delivery tools in the future.

We thank Mr. Kazuyuki Ito for valuable advice and help with proofreading. This work was supported by Medical Techniques Promotion Research Grant from the Ministry of Health, Labour and Welfare of Japan (H14-nano-004, Kenji Yamamoto).

References

1) Aglipay, J.A., Lee, S.W., Okada, S., Fujiuchi, N., Ohtsuka, T., Kwak, J.C., Wang, Y., Johnstone, R.W., Deng, C., Qin, J., and Ouchi, T. 2003. Oncogene **22**: 8931–8938.
2) Akerman, M.E., Chan, W.C., Laakkonen, P., Bhatia, S.N., and Ruoslahti, E. 2002. Nanocrystal targeting *in vivo*. Proc. Natl. Acad. Sci. U.S.A. **99**: 12617–12621.
3) Ballou, B., Lagerholm, B.C., Ernst, L.A., Bruchez, M.P., and Waggoner, A.S. 2004. Noninvasive imaging of quantum dots in mice. Bioconjugate Chem. **15**: 79–86.
4) Bruchez, M., Jr., Moronne, M., Gin, P., Weiss, S., and Alivisatos, A.P. 1998. Semiconductor nanocrystals as fluorescent biological labels. Science **281**: 2013–2016.
5) Chan, W.C., and Nie, S. 1998. Quantum dot bioconjugates for ultrasensitive nonisotopic detection. Science **281**: 2016–2018.
6) Dabboussi, B.O., Rodriguez-Viejo, J., Mikulec, F.V., Hein, J.R., Mattoussi, H., Ober, R., Jensen, K.F., and Bawendi, M.G. 1997. (CdSe)ZnS core-shell quantum dots; synthesis and characterization of size series of highly luminescent nanocrystallites. J. Phys. Chem. **101**: 9463–9475.

7) Dubertret, B., Skourides, P., Norris, D.J., Noireaux, V., Brivanlou, A.H., and Libchaber, A. 2002. *In vivo* imaging of quantum dots encapsulated in phospholipid micelles. Science **298**: 1759–1762.
8) Gao, X., Chan, W.C., and Nie, S. 2002. Quantum-dot nanocrystals for ultrasensitive biological labeling and multicolor optical encoding. J. Biomed. Opt. **7**: 532–537.
9) Gao, X., Cui, Y., Levenson, R.M., Chung, L.W.K., and Nie, S. 2004. *In vivo* cancer targeting and imaging with semiconductor quantum dots. Nat. Biotechnol. **22**: 969–976.
10) Gerion, D., Pinaud, F., Williams, S.C., Parak, W.J., Zanchet, D., Weiss, S., and Alivisatos, A.P. 2001. Synthesis and properties of biocompatible water-soluble silica-coated CdSe/ZnS semiconductor quantum dots. J. Phys. Chem. **105**: 8861–8871.
11) Goldman, E.R., Anderson, G.P., Tran, P.T., Mattoussi, H., Charles, P.T., and Mauro, J.M. 2002. Conjugation of luminescent quantum dots with antibodies using an engineered adaptor protein to provide new reagents for fluoroimmunoassays. Anal. Chem. **74**: 841–847.
12) Gorlich, D., and Mattaj, I.W. 1996. Nucleocytoplasmic transport. Science **271**: 1513–1518.
13) Haggie, P.M., and Verkman, A.S. 2002. Diffusion of tricarboxylic acid cycle enzymes in the mitochondrial matrix *in vivo*. Evidence for restricted mobility of a multienzyme complex. J. Biol. Chem. **277**: 40782–40788.
14) Hanaki, K., Momo, A., Oku, T., Komoto, A., Maenosono, S., Yamaguchi, Y., and Yamamoto, K. 2003. Semiconductor quantum dot/albumin complex is a long-life and highly photostable endosome marker. Biochem. Biophys. Res. Commun. **302**: 496–501.
15) Hines, M.A., and Guyot-Sionnest, P. 1996. Synthesis and characterization of strongly luminescing ZnS-capped CdSe nanocrystals. J. Phys. Chem. **100**: 468–471.
16) Hoshino, A., Fujioka, K., Oku, T., Suga, M., Sasaki, Y.F., Ohta, T., Yasuhara, M., Suzuki, K., and Yamamoto, K. 2004. Physicochemical properties and cellular toxicity of nanocrystal quantum dots depend on their surface modification. Nano Lett. **4**: 2163–2169.
17) Hoshino, A., Hanaki, K., Suzuki, K., and Yamamoto, K. 2004. The applications T-lymphoma labeled with fluorescent quantum dots to cell trafficking markers in a mouse body. Biochem. Biophys. Res. Commun. **314**: 46–53.
18) Ishii, D., Kinbara, K., Ishida, Y., Ishii, N., Okochi, M., Yohda, M., and Aida, T. 2003. Chaperonin-mediated stabilization and ATP-triggered release of semiconductor nanoparticles. Nature **423**: 628–632.
19) Jaiswal, J.K., Mattoussi, H., Mauro, J.M., and Simon, S.M. 2003. Long-term multiple color imaging of live cells using quantum dot bioconjugates. Nat. Biotechnol. **21**: 47–51.
20) Johnson, L.V., Walsh, M.L., and Chen, L.B. 1980. Localization of mitochondria in living cells with rhodamine 123. Proc. Natl. Acad. Sci. U.S.A. **77**: 990–994.
21) Kaether, C., and Gerdes, H.H. 1995. Visualization of protein transport along the secretory pathway using green fluorescent protein. FEBS Lett. **369**: 267–271.
22) Kaul, Z., Yaguchi, T., Kaul, S.C., Hirano, T., Wadhwa, R., and Taira, K. 2003. Mortalin imaging in normal and cancer cells with quantum dot immuno-conjugates. Cell Res. **13**: 503–507.
23) Larson, D.R., Zipfel, W.R., Williams, R.M., Clark, S.W., Bruchez, M.P., Wise, F.W., and Webb, W.W. 2003. Water-soluble quantum dots for multiphoton fluorescence imaging *in vivo*. Science **300**: 1434–1436.
24) Lidke, D.S., Nagy, P., Heintzmann, R., Arndt-Jovin, D.J., Post, J.N., Grecco, H.E., Jares-Erijman, E.A., and Jovin, T.M. 2004. Quantum dot ligands provide new insights into erbB/HER receptor-mediated signal transduction. Nat. Biotechnol. **22**: 198–203.
25) Matsushita, M., Tomizawa, K., Moriwaki, A., Li, S.T., Terada, H., and Matsui, H.J. 2001. A high-efficiency protein transduction system demonstrating the role of PKA in long-lasting long-term potentiation. J. Neurosci. **21**: 6000–6007.
26) Mattaj, I.W., and Englmeier, L. 1998. Nucleocytoplasmic transport: the soluble phase. Annu. Rev. Biochem. **67**: 265–306.
27) Mattoussi, H., Mauro, J.M., Goldman, E.R., Anderson, G.P., Sundar, V.C., Mikulec, F.V., and Bawendi, M.G. 2000. Self-assembly of CdSe-ZnS quantum dot bioconjugates using an engineered recombinant protein. J. Am. Chem. Soc. **122**: 12142–12150.
28) Medintz, I.L., Clapp, A.R., Mattoussi, H., Goldman, E.R., Fisher, B., and Mauro, J.M. 2003. Self-assembled nanoscale biosensors based on quantum dot FRET donors. Nat. Mater. **2**: 630–639.
29) Osaki, F., Kanamori, T., and Sando, S., Sera, T., and Aoyama, Y. 2004. Quantum dot conjugated sugar ball and its cellular uptake. On the size effects of endocytosis in the subviral region. J. Am. Chem. Soc. **126**: 6520–6521.
30) Pinaud, F., King, D., Moore, H.P., and Weiss, S. 2004. Bioactivation and cell targeting of semiconductor CdSe/ZnS nanocrystals with phytochelatin-related peptides. J. Am. Chem. Soc. **126**: 6115–6123.
31) Rizzuto, R., Brini, M., Pizzo, P., Murgia, M., and Pozzan, T. 1995. Chimeric green fluorescent protein as a tool for visualizing subcellular organelles in living cells. Curr. Biol. **5**: 635–642.
32) Rosenthal, S.J., Tomlinson, I., Adkins, E.M., Schroeter, S., Adams, S., Swafford, L., McBride, J., Wang, Y., DeFelice, L.J., and Blakely, R.D. 2002. Targeting cell surface receptors with ligand-conjugated nanocrystals. J. Am. Chem. Soc. **124**: 4586–4594.
33) Shibahara, A., Hoshino, A., Hanaki, K., Suzuki, K., and Yamamoto, K. 2004. On the cyto-toxicity caused by quantum dots. Microbiol. Immunol. **48**: 669–675.
34) Shubeita, G.T., Sekatskii, S.K., Dietler, G., Potapova, I., Mews, A., and Basch, T. 2003. Scanning near-field optical microscopy using semiconductor nanocrystals as a local fluorescence and fluorescence resonance energy transfer source. J. Microsc. **210**: 274–278.
35) Smith, A.M., Gao, X., and Nie, S. 2004. Quantum-dot nanocrystals for *in-vivo* molecular and cellular imaging. Photochem. Photobiol. (in press).
36) Su, X.L., and Li, Y. 2004. Quantum dot biolabeling coupled with immunomagnetic separation for detection of *Escherichia coli* O157:H7. Anal. Chem. **76**: 4806–4810.
37) Taguchi, T., Shimura, M., Osawa, Y., Suzuki, Y., Mizoguchi, I., Niino, K., Takaku, F., and Ishizaka, Y. 2004.

Nuclear trafficking of macromolecules by an oligopeptide derived from Vpr of human immunodeficiency virus type-1. Biochem. Biophys. Res. Commun. **320**: 18–26.

38) Voura, E.B., Jaiswal, J.K., Mattoussi, H., and Simon, S.M. 2004. Tracking metastatic tumor cell extravasation with quantum dot nanocrystals and fluorescence emission-scanning microscopy. Nat. Med. **10**: 993–998.

39) Wu, H.Y., Tomizawa, K., Matsushita, M., Lu, Y.F., Li, S.T., and Matsui, H. 2003. Poly-arginine-fused calpastatin peptide, a living cell membrane-permeable and specific inhibitor for calpain. Neurosci. Res. **47**: 131–135.

40) Wu, X., Liu, H., Liu, J., Haley, K.N., Treadway, J.A., Larson, J.P., Ge, N., Peale, F., and Bruchez, M.P. 2003. Immunofluorescent labeling of cancer marker Her2 and other cellular targets with semiconductor quantum dots. Nat. Biotechnol. **21**: 41–46.

41) Xu, H., Sha, M.Y., Wong, E.Y., Uphoff, J., Xu, Y., Treadway, J.A., Truong, A., O'Brien, E., Asquith, S., Stubbins, M., Spurr, N.K., Lai, E.H., and Mahoney, W. 2003. Multiplexed SNP genotyping using the Qbead system: a quantum dot-encoded microsphere-based assay. Nucleic Acids Res. **31**: 43.

Non-glycosylphosphatidylinositol (GPI)-anchored recombinant prion protein with dominant-negative mutation inhibits PrP^{Sc} replication *in vitro*

Hitaru Kishida[1,2], Yuji Sakasegawa[1,3], Kota Watanabe[1,3], Yoshio Yamakawa[4], Masahiro Nishijima[4], Yoshiyuki Kuroiwa[2], Naomi S. Hachiya[1,3] and Kiyotoshi Kaneko[1,3]

1. Department of Cortical Function Disorders, National Institute of Neuroscience, National Center of Neurology and Psychiatry, Kodaira, Tokyo, Japan
2. Department of Neurology, Yokohama City University, Yokohama, Japan
3. Core Research for Evolutional Science and Technology (CREST), Japan Science and Technology Corporation, Kawagoe, Saitama, Japan
4. Department of Biochemistry and Cell Biology, National Institute of Infectious Diseases, Tokyo, Japan

KEY WORDS: *recombinant prion protein (rPrP), dominant negatives, Q218K, quinacrine, glycosylphosphatidylinositol (GPI)-anchor, lipid rafts, Creutzfeldt-Jakob disease (CJD)*

ABBREVIATIONS: *PrP = prion protein, GPI = glycosylphosphatidylinositol, CJD = Creutzfeldt-Jakob disease, rPrP = recombinant prion protein, EC_{50} = 50% effective concentration, EC_{99} = 99% effective concentration, PrP^{C} = host-encoded cellular prion protein, PrP^{Sc} = abnormal protease-resistant pathogenic prion protein, TSE = transmissible spongiform encephalopathy, BSE = bovine spongiform encephalopathy, IPTG = Isopropyl-β-D-thiogalactopyranoside, β-ME = β-mercaptoethanol, PMSF = Phenylmethylsulfonyl fluoride, PBS = phosphate buffer saline, PK = proteinase K, WST-8 = 2- (2-methoxy-4-nitrophenyl)- 3- (4-nitrophenyl)- 5- (2,4-disulfophenyl)- 2H- tetrazolium, monosodium salt, SPR = surface plasmon resonance, PIPLC = phosphatidyl-inositol specific phospholipase C*

Abstract

Dominant-negative mouse prion protein (PrP) with a lysine mutation at codon 218 (Q218K) is known to inhibit prion replication. In order to gain further mechanistic insight into such dominant negative inhibition, non-glycosylphosphatidylinositol (GPI)-anchored recombinant PrP with Q218K (rPrP-Q218K) was investigated. When applied into scrapie-infected mouse neuroblastoma (ScN2a) cells, rPrP-Q218K but not wild-type rPrP (rPrP-WT) exclusively inhibited abnormal protease-resistant pathogenic isoform (PrP^{Sc}) replication without reducing the viability of the cells. It was even more efficient than quinacrine, which has already been prescribed for sporadic Creutzfeldt-Jakob disease (CJD) patients; 50% effective concentration (EC_{50}) = 0.20 μM, 99% effective concentration (EC_{99}) = 0.86 μM vs. EC_{50} = 0.45 μM, EC_{99} = 1.5 μM. Besides, no apparent cell damage was observed at the concentration of up to 4.3 μM (100 μg/ml). In combination treatment with 0.43 μM (10 μg/ml) of rPrP-Q218K, EC_{99} of quinacrine was decreased from 1.5 μM to 0.5 μM, and the cell viability was recovered from 50% to over 90% as inversely proportional to the concentration of quinacrine. Such combination could alleviate the side effects of quinacrine by reducing its effective concentration without changing or even acceleration the inhibition efficacy. Since homogeneous, high-quality rPrPs could be easily prepared from Escherichia coli in large quantities, rPrP-Q218K is a good candidate for a prion replication antagonist.

Correspondence: Dr. Kiyotoshi Kaneko, MD, Department of Cortical Function Disorders, National Institute of Neuroscience, National Center of Neurology and Psychiatry, 4-1-1 Ogawahigashi Kodaira, Tokyo 187-8502, Japan
Tel: 81-42-346-1718 Fax: 81-42-346-1748 E-mail: kaneko@ncnp.go.jp

Submitted: July 14, 2003 Revision Accepted: October 22, 2003

DOI: 10.1080/13506120410001689634

Introduction

Human prion disease or transmissible spongiform encephalopathy (TSE), such as sporadic Creutz-feldt-Jakob disease (CJD) and variant CJD transmitted from bovine spongiform encephalopathy (BSE) constitutes a group of invariably fatal neurodegenerative disorders[1,2]. Prion protein (PrP) consists of two isoforms, one is a host-encoded cellular isoform (PrP^{C}) and the other is an abnormal protease-resistant pathogenic isoform (PrP^{Sc}). The latter is a causative agent of prion disease. PrP^{Sc} stimulates the conversion of PrP^{C} into nascent PrP^{Sc}, and the accumulation of PrP^{Sc} leads to the central nervous system (CNS) dysfunction and neuronal degeneration[3].

A human polymorphic lysine variant at codon 219 (E219K) in the Japanese population, known to render humans resistant to sporadic CJD[4,5], acts as a dominant negative in scrapie-infected mouse neuroblastoma (ScN2a) culture cells after gene transfection[6,7] and transgenic mice expressing lysine at codon 218 in mouse PrP (mouse Q218K, which corresponds to human E219K)[8]. Of note, such a genetic population with E219K and the transgenic mice with Q218K complete their life span with no apparent phenotypic abnormality[5,8].

We now demonstrate that administration of non-glycosylphosphatidylinositol (GPI)-anchored recombinant PrP (rPrP) with Q218K mutation (rPrP-Q218K) but not wild-type rPrP (rPrP-WT) exclusively inhibited the PrP^{Sc} formation in ScN2a cells, even more efficiently than quinacrine, which has already been prescribed for CJD patients, and no apparent cell damage was observed up to 5-fold higher concentrations of a 99% effective concentration (EC_{99}). When combined, rPrP-Q218K efficiently reduced the effective dosage of quinacrine, and thus rendered ScN2a culture cells more viable. Such a combination could alleviate the side effects of quinacrine by reducing its effective concentration without changing or even accelerating the inhibition efficacy. Since homogeneous, high-quality rPrP could be easily prepared from *Escherichia coli* in large quantities, rPrP-Q218K might be a good candidate as a prion replication antagonist.

Materials and methods

Expression plasmid construction

The gene, mouse (Mo) PrP(23-230), coding for residues 23-230 of mouse PrP was PCR-amplified from mouse brain cDNA using the oligonucleotide primers (5′-GGAATTCACCATGAAAAAGCGGCCAAAGCCTGG-AGGG-3′ and 5′-CCGCTCGAGTCAGGATCTTCTCC-CGTCGTAATAGGC-3′) and cloned via *EcoRI* and *XhoI* sites into the plasmid pBluescript II SK(+) (Stratagene, La Jolla, CA). The genes for 3F4-tagged MoPrP (MHM2PrP) were also cloned using PCR amplification from pSPOX-MHM2PrP[9,10] as above. The Q218K mutation was generated by PCR-directed mutagenesis using primers (5′-ATGTGCGTCACCCAGTACAAAAAGGA-GTCC-3′ and 5′-ATAGGCCTGGGACTCCTTTTTG-TACTGGGT-3′). The DNA fragments were cloned into a modified pET-11a (Invitrogen, Carlsbad, CA), pEY2, of which *EcoRI* and *XhoI* sites were introduced as multi-cloning sites, via *EcoRI* and *XhoI* sites.

Purification of recombinant prion proteins (rPrPs)

The rPrPs were expressed as inclusion bodies in the *E. coli* BL21(DE3) (Stratagene) in the presence of 0.1 mM Isopropyl-β-D-thiogalactopyranoside (IPTG). The inclusion bodies were collected from sonicated lysates by centrifugation at 27,000 × g for 10 min, washed three times in Buffer A (2 M urea, 50 mM Tris-HCl, pH 7.5, 150 mM NaCl, 2 mM β-mercaptoethanol (β-ME), 0.5 mM Phenylmethylsulfonyl fluoride (PMSF)), and solubilized in Buffer B (8 M urea, 25 mM Tris-HCl, pH 7.5, 2 mM β-ME, 0.5 mM PMSF). After centrifugation (200,000 × g, 30 min), the supernatant was applied to a CM-Sepharose column (Amersham Bioscience, Piscataway, NJ), washed with Buffer B containing 100 mM NaCl and eluted with Buffer B containing 150 mM NaCl. The eluate containing rPrP was applied to an Ni-NTA agarose column (Qiagen, Valencia, CA), washed with Buffer B containing 5 mM imidazole and eluted with Buffer B containing 200 mM imidazole. The eluate was diluted 10-fold 1 M arginine-HCl, pH 8.0, 1 mM reduced glutathione, 0.8 mM oxidized glutathione and incubated at 4°C overnight. After incubation at 37°C for 10 min, the refolded recombinant proteins were concentrated and buffer-changed into phosphate buffer saline (PBS) by Ultrafree-15 10K NMWL (Millipore, Billerica, MA). Concentrations of rPrP were calculated by the absorbance at 280 nm with specific absorbance unit ($A_{280nm,\ 1mg/ml,\ 1cm}$) of 2.70.

Inhibition assay of PrP^{Sc} accumulation in ScN2a cells

ScN2a cells were grown and maintained as described[11]. Twenty-four hours after splitting, cells were incubated in a fresh medium containing the appropriate concentration of rPrP and/or quinacrine (Sigma, St. Louis, MO) or the same volume of PBS as a negative control and incubated for 3 days. Quinacrine was dissolved in PBS. Cell lysis and proteinase K (PK) digestion were performed as described[12]. PK-insoluble pellets and PK-undigested samples were subjected to 12% SDS-PAGE and Western blotting using standard procedure. Anti-PrP

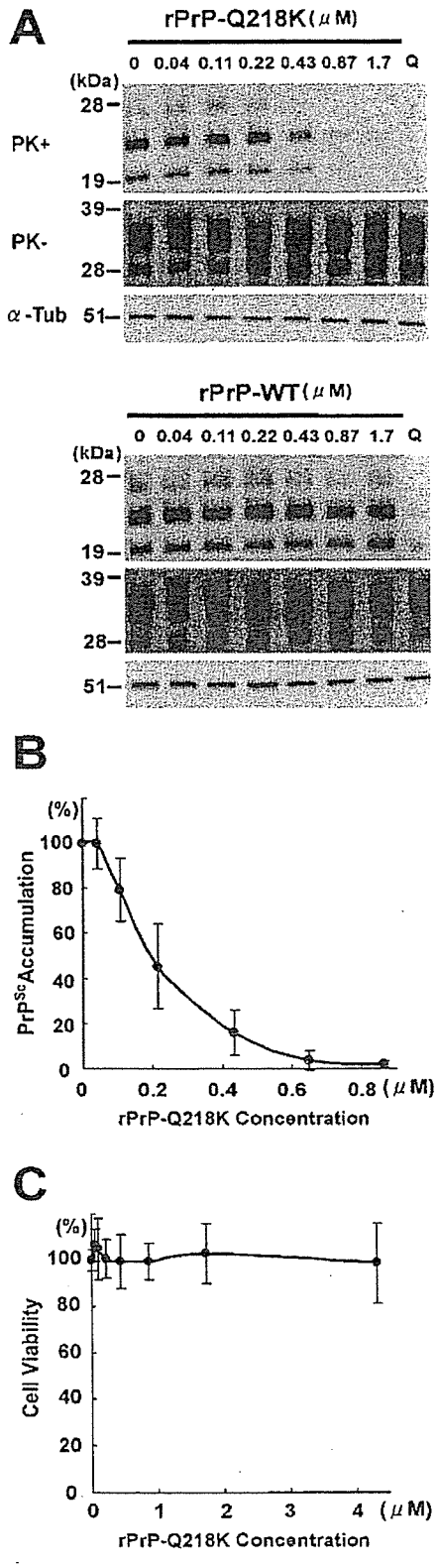

monoclonal antibody (mAb) 6H4 (1:5000; Prionics, Schlieren, Switzerland) or α-tubulin mAb (1 : 10000; DM1A, Sigma) was used as the primary antibody, and horseradish peroxydase-conjugated anti-mouse IgG (1 : 5000; Cappel, West Chester, PA) was used as the secondary antibody. Immunodecorated bands were visualized by the ECL-plus (Amersham Bioscience). For evaluating the accumulation of PrP^{Sc}, the PK-resistant bands were quantified by densitometry (LAS-1000; Fujifilm, Tokyo, Japan). Average values of at least three independent experiments were plotted as percentage of the amount of PrP^{Sc} found in equivalent untreated ScN2a cells on the day of collection.

Cytotoxicity assays

The cytotoxicity of rPrP and quinacrine in ScN2a cells was evaluated by the WST-8 assay (Cell Counting Kit-8, Dojindo Lab, Kumamoto, Japan) measuring the formation of a yellow color formazan dye produced by dehydrogenase activities in viable cells from 2- (2-methoxy-4-nitrophenyl)- 3- (4-nitrophenyl)- 5- (2,4-disulfophenyl)- 2H- tetrazolium, monosodium salt (WST-8). ScN2a cells (4×10^{3} cells/well) were cultured at 37°C for 24 h in 96-well plates, incubated in the medium containing the appropriate concentration of drugs for 48 h and were subjected to WST-8 assay according to the manufacturer's protocol.

FIGURE 1: Dose-dependent inhibition of PrP^{Sc} formation in ScN2a cells with rPrP-Q218K. (A) PrP^{Sc} signals in ScN2a culture cells are compared by immunoblotting in the presence of rPrP-Q218K or rPrP-WT at 0 – 1.7 μM (0 - 40 μg/ml). (0) represents untreated cells, and (Q) represents positive controls treated with 1.5 μM of quinacrine. PrP^{Sc} is detected with anti-PrP mAb (6H4) after proteinase K (PK) digestion (20 μg/ml, 1 h, 37°C, 1st row), and total PrP (PrP^{C} and PrP^{Sc}) is detected without PK digestion (2nd row). After incubation with rPrP-Q218K, PrP^{Sc} in ScN2a cells is reduced in a dose-dependent manner, whereas the administration of rPrP-WT by up to 1.7 μM (40 μg/ml) does not change PrP^{Sc} formation. Total PrP remains unchanged in both treatments. The same undigested cell lysates are stained with αtubulin mAb (DM1A, Sigma, St. Louis, MO). (B) Densitometric measurements of PrP^{Sc} signals in panel A. All data represent the mean values (± SD) from at least three independent experiments. (C) Cell viability is determined by the WST-8 assay, in which the absorbance values indicate the yield of colored formazan in proportion to total number of viable cells. Each point represents the mean absorbance value (± SD) calculated from four sets of experimental data. Up to 4.3 μM (100 μg/ml) of rPrP-Q218K doesn't reduce the viability of ScN2a cells.

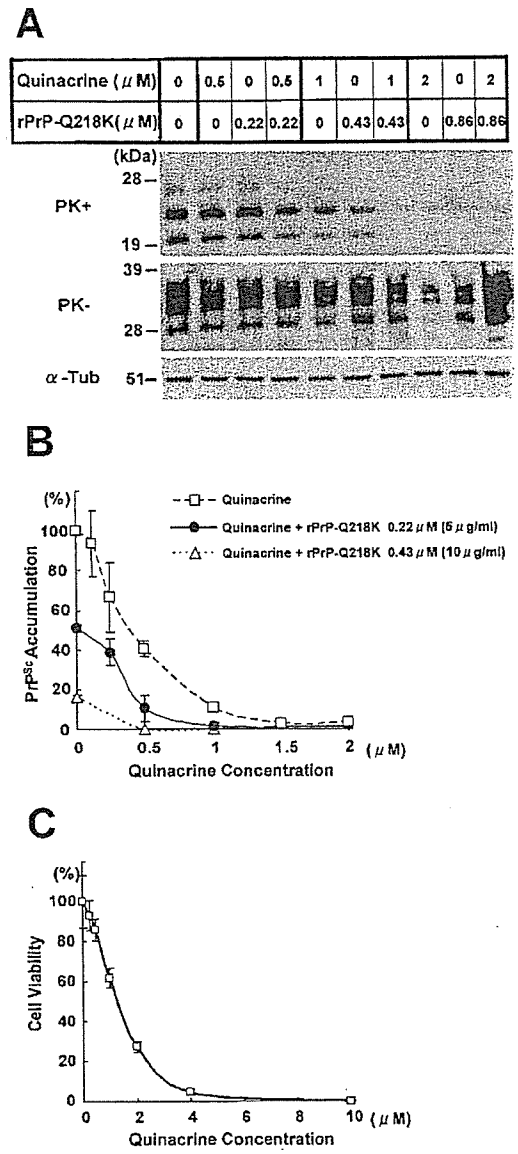

FIGURE 2: Additive inhibition of PrP^{Sc} formation by the combination of rPrP-Q218K and quinacrine. (A) PrP^{Sc} signals in ScN2a cells are compared by immunoblotting in the presence of quinacrine and/or rPrP-Q218K (see legend to Figure. 1A). PrP^{Sc} level in ScN2a cells is additively reduced. (B) Densitometric measurements of PrP^{Sc} signals in panel A (see legend to Figure. 1B). Open squares, quinacrine; filled circles, quinacrine with 0.22 μM (5 μg/ml) of rPrP-Q218K; open triangles, quinacrine with 0.43 μM (10 μg/ml) of rPrP-Q218K. The inhibition on PrP^{Sc} formation with quinacrine with rPrP-Q218K is more effective than that of quinacrine alone. (C) Cell viability is determined by the WST-8 assay (see legend to Figure. 1C). The treatment of quinacrine damages the cell viability in a dose-dependent manner.

Immunofluorescent microscopy

For indirect immunofluorescence analysis, mouse neuroblastoma (N2a) cells grown on glass cover slips in the presence of 0.43 μM (10 μg/ml) of rPrP with 3F4 epitope (MHM2 rPrP) for 3 h were rinsed with PBS without Ca^{2+} and Mg^{2+} (PBS(−)) and then fixed with 2% formalin in 70% PBS(−) for 15 min at room temperature. After four washes, the fixed cells were incubated 10% FBS in PBS(−) for 30 min at room temperature. They were then incubated for 1 h at room temperature with anti-SHaPrP 3F4 mAb (1:200; Sigma) and anti-asialo-GM1 antibody (1:200, CALBIOCHEM, La Jolla, CA) as a marker of rafts. After four washes with PBS (−), the cells were incubated with Alexa 488 Fluor-conjugated goat anti-mouse IgG (1:500, Molecular Probes, Eugene, OR) and Alexa 594 Fluor-conjugated goat anti-rabbit IgG (1:100, Molecular Probes) for 1 h at room temperature. The cells were washed 4 times with PBS(−) and mounted with SLOW FADE (Molecular Probes) and observed using Delta Vision Microscope Systems (Applied Precision, LLC).

Surface plasmon resonance (SPR) measurement

A BIAcore 3000 system (BIAcore AB, Uppsala, Sweden) was used to analyze molecular interactions by means of SPR. rPrP-WT at 500 μg/ml was diluted 1:10 with 10 mM sodium acetate buffer at pH 6.0 and immobilized to a sensor chip CM5 (carboxymethylated dextran surface) using amine coupling according to the manufacture's instructions. Samples for analyte proteins were diluted ($3.2 \times 10^{-2 \sim 0}$ μg/ml) in the running buffer (10 mM HEPES-KOH, pH 7.4, 150 mM NaCl, 3 mM EDTA, 0.005% Surfactant P20), and injected over the surface at 4°C with a flow rate of 20 μl/min. Each sensorgram was subtracted for the response observed in the control flow cell containing a blank surface and results were analyzed by using BIA evaluation SPR kinetic software (BIAcore).

Results

Purified rPrP-Q218K or rPrP-WT was added into the culture media of ScN2a cells at the designated concentrations and incubated for 3 days (see Materials and methods). Ultracentrifugation using a sucrose density gradient revealed that these rPrPs were monomeric (data not shown). While PrP^{Sc} formation was not altered by up to 1.7 μM (40 μg/ml) of rPrP-WT (Figure 1A), it was dramatically reduced in rPrP-Q218K-treated ScN2a cells; 50% effective concentration (EC_{50}) was 0.19 μM (4.5 μg/ml) and EC_{99} was 0.86 μM (20 μg/ml) (Figure 1B) in a concentration-dependent manner (Figures 1A, 1B). Of